Combined-probability space and certainty or uncertainty relations for a finite-level quantum system

Arun Sehrawat*

Department of Physical Sciences, Indian Institute of Science Education & Research (IISER) Mohali, Sector 81 SAS Nagar, Manauli PO 140306, Punjab, India

(Received 12 April 2017; published 7 August 2017)

The Born rule provides a probability vector (distribution) with a quantum state for a measurement setting. For two settings, we have a pair of vectors from the same quantum state. Each pair forms a combined-probability vector that obeys certain quantum constraints, which are triangle inequalities in our case. Such a restricted set of combined vectors, called the combined-probability space, is presented here for a d-level quantum system (qudit). The combined space is a compact convex subset of a Euclidean space, and all its extreme points come from a family of parametric curves. Considering a suitable concave function on the combined space to estimate the uncertainty, we deliver an uncertainty relation by finding its global minimum on the curves for a qudit. If one chooses an appropriate concave (or convex) function, then there is no need to search for the absolute minimum (maximum) over the whole space; it will be on the parametric curves. So these curves are quite useful for establishing an uncertainty (or a certainty) relation for a general pair of settings. We also demonstrate that many known tight certainty or uncertainty relations for a qubit can be obtained with the triangle inequalities.

DOI: 10.1103/PhysRevA.96.022111

I. INTRODUCTION

Every setting for a measurement of a quantum system can be completely specified by an orthonormal basis of the system's Hilbert space. Identical systems can be independently prepared in a (pure) state ρ such that, every time, we get a definite outcome when a system is measured in a setting a. If we change a to a physically distinct setting, b, then we observe—sometimes one and sometimes the other—multiple outcomes. In other words, there the probability is 1 for an outcome in setting a, whereas none of the probabilities is 1 in setting b. Of course, in any setting, all the probabilities are nonnegative numbers that sum up to 1. Apart from that, the probability vectors (distributions) $\vec{p}$ and $\vec{q}$—associated with the two settings a and b, respectively—must follow certain constraints, called *quantum constraints* (QCs), together.

Historically, such QCs are expressed in terms of uncertainty relations (URs) by taking Hermitian operators rather than orthonormal bases. A UR is an inequality, $\mathsf{c}(a,b,\rho) \leqslant \mathsf{u}(a,b,\rho)$, between two real-valued functions: the uncertainty measure u and its lower bound c. In 1927, Heisenberg introduced the first UR [1,2] (derived by Weyl in [3]) for the position and momentum operators. Different aspects of his seminal work are reviewed in [4]. Robertson [5] generalized Heisenberg's relation for an arbitrary pair of operators by employing the standard deviation as a measure of the uncertainty. In Robertson's UR, the lower bound c is a function of the state ρ. Deutsch criticized it and introduced a new UR [6] for a finite-dimensional state space by taking the entropy as a measure of the uncertainty. He achieved a state-independent $\mathsf{c}(a,b)$. Later, a better lower bound was conjectured by Kraus [7] and then proved by Maassen and Uffink [8]. Such URs—known as entropy URs—are reviewed in [9–11].

Throughout this article, we consider d-level quantum systems (qudits) and projective measurements. Our primary objective is to study a set of combined-probability vectors $(\vec{p},\vec{q})$, called the *combined-probability space*, where every vector respects certain, if not all, QCs. Here the elemental QCs are the triangle inequalities (TIs) between *quantum angles*, and the certainty or uncertainty relations emerge from them. As an angle between a pair of kets—called a quantum angle—is a metric over the set of all pure states [12], we own the TIs. Landau and Pollak obtained a single TI [13] of this kind for continuous-time signals and provided a classical UR (see also Sec. 8 in [14]).

In Sec. II, we present the combined space, which is a compact convex subset of the $2d$-dimensional real vector space $\mathbb{R}^{2d}$. Thanks to the Krein-Milman theorem (see Theorem 3.3.5 and Appendix A.3 in [15]), every compact convex subset of $\mathbb{R}^{2d}$ can be generated by the convex combinations of its extreme points. As a principal result, we provide a family of *parametric curves* in Sec. II, which represents all the extreme points of the combined space. In the case of $d = 2$, all the parametric curves form an ellipse, and the same ellipse also appears in [16–18] as a special case.

An uncertainty measure, $\mathsf{u}(a,b,\rho) \equiv \mathsf{u}(\vec{p},\vec{q})$, should be a concave function on the combined-probability space, argued at the beginning of Sec. III. The concavity of u ensures that its global minimum c will occur on the parametric curves (extreme points) of the space (see Theorem 3.4.7 and Appendix A.3 in [15]). Hence, one can exploit these curves to obtain a UR, rather easily, for her or his choice of u and, of course, for general measurement settings a and b.

In Sec. III, we choose a concave, thus uncertainty, measure, $\mathsf{u}(\vec{p},\vec{q})$. The significance of our choice lies in the fact that u is again a concave function on every parametric curve (that is, as a function of the parameter). Therefore its absolute minimum c will occur nowhere but at the endpoint(s) of these curves. A simple three-step procedure is carried out to find the lower bound $\mathsf{c} \leqslant \mathsf{u}$ for an arbitrary pair $\{a,b\}$ of settings and for a finite d. One can employ an ordinary computer to run the procedure. Besides, c is presented in analytic forms for $d = 2$ and 3 and in the case of mutually unbiased bases (MUBs) [19]. References [7,17] and [20–24] report URs particularly for MUBs. At the end of Sec. III, we provide another uncertainty

*aruns@iisermohali.ac.in

measure that is also concave on all the parametric curves, so the whole analysis given before for u can be straightforwardly applied to this measure.

If a suitable concave function can be a measure of the uncertainty, then an appropriate convex function will be a measure of the certainty. In Sec. IV, we pick some other concave and convex functions and exhibit that the tight uncertainty and certainty relations given in [6,8,17] and [25–32] for a qubit can be achieved with the TIs that specify the ellipse. We conclude the article with Sec. V.

The appendixes are reserved for certain technical details and proofs: The TIs are derived in Appendix A. It is shown in Appendix B that the combined space is a compact convex set. The parametric curves are explicitly obtained in Appendix D with the help of Appendix C.

II. QUANTUM CONSTRAINTS AND COMBINED-PROBABILITY SPACE

In quantum theory, observables are represented by Hermitian operators. If such an operator is degenerate, then it possesses more than one eigenbases, and some of them can represent physically different measurement setups. Hence, "a measurement in an orthonormal basis" of the underlying Hilbert space is more precise than "a measurement of an operator" (see Chap. 7 in [33]). In fact, measurements in a basis $\mathcal{B}_a$ measure all the operators whose eigenbasis is $\mathcal{B}_a$. Moreover, Deutsch pointed out that a measure of uncertainty for a discrete observable must depend not on its eigenvalues, but on its eigenbasis [6]. With all these considerations, we choose orthonormal bases instead of Hermitian operators to specify different projective measurements for a qudit.

We begin with two orthonormal bases,

$$\mathcal{B}_a := \{|a_i\rangle\}_{i=1}^d \quad \text{and} \quad \mathcal{B}_b := \{|b_j\rangle\}_{j=1}^d, \tag{1}$$

of a d-dimensional Hilbert space $\mathscr{H}_d$ to depict the two measurement settings a and b, respectively. In this paper, all certainty and uncertainty relations are *preparation* certainty and uncertainty relations that are applicable in the following experimental scheme.

> A number of independent qudits are identically prepared in a quantum state ρ. Then half of them are measured in the basis $\mathcal{B}_a$ and the rest in $\mathcal{B}_b$, one by one. (2)

Peres used a similar scenario on page 93 of his book [33] to interpret the position-momentum UR. In proposal (2), clearly, the two measurements have no influence on each other whatsoever.

Throughout the text, we assume that ρ is a pure quantum state $|\psi\rangle\langle\psi|$ so that we can associate angles, (4), and TIs, (12), with the state vector $|\psi\rangle$. However, every certainty and uncertainty relation presented in this paper is applicable to every qudit's state [see the text around (39)].

The state $\rho = |\psi\rangle\langle\psi|$ provides two probability distributions for the two measurement settings [given in (1)] by the Born rule:

$$p_i = |\langle a_i|\psi\rangle|^2 \quad \text{and} \quad q_j = |\langle b_j|\psi\rangle|^2 \tag{3}$$

are the probabilities of getting outcome a_i in setting a and outcome b_j in setting b, respectively. Next, we present the quantum angles:

$$\alpha_i = \arccos|\langle a_i|\psi\rangle| \quad \text{and} \quad \beta_j = \arccos|\langle b_j|\psi\rangle| \tag{4}$$

are the angles between $|\psi\rangle$ and $|a_i\rangle$ and between $|\psi\rangle$ and $|b_j\rangle$, respectively. Throughout this article, we consider only the principal values $[0,\pi]$ of the (multivalued) arccos function. With (3) and (4), one can recognize that the absolute value of the inner product establishes a one-to-one correspondence between the angles—which belong to $[0,\frac{\pi}{2}]$—and the probabilities—which lie in $[0,1]$.

Related to the a setting, every probability vector $\vec{p} := (p_1,\ldots,p_d)$ satisfies

$$\sum_{i=1}^d p_i = 1, \tag{5}$$

$$0 \leqslant p_i \quad \text{for all} \quad 1 \leqslant i \leqslant d, \tag{6}$$

and the collection of all such vectors constitutes a probability space Ω_a. Similarly, Ω_b is—related to the basis $\mathcal{B}_b$—defined by the constraints

$$\sum_{j=1}^d q_j = 1 \quad \text{and} \tag{7}$$

$$0 \leqslant q_j \quad \text{for all} \quad 1 \leqslant j \leqslant d. \tag{8}$$

Equations (5) and (7) state that all the probabilities add up to 1, and inequalities (6) and (8) tell us that probabilities are nonnegative numbers. Both Ω_a and Ω_b are—the standard $(d-1)$ simplexes—compact convex subsets of the d-dimensional real vector space $\mathbb{R}^d$, and their Cartesian product $\Omega := \Omega_a \times \Omega_b$ is a compact convex subset of $\mathbb{R}^{2d}$ (see Appendix B). Basically, Ω is determined by conditions (5)–(8).

Performing measurements on every qudit using a single setting, say a, is like throwing a d-sided dice, every time. The vector $\vec{p}$ alone is limited by (5) and (6), which specify Ω_a, which is also the probability space of a d-sided die. However, the experimental scheme, (2), is not similar to throwing one of two d-sided dice at a time, although Ω is the probability space of two dice: every pure or mixed state of a qudit gives a unique pair $(\vec{p},\vec{q}) \in \Omega$ by the Born rule [see (3) and (39)], but *not every* pair $(\vec{p},\vec{q}) \in \Omega$ has a quantum state. For example, if $|\langle a_i|b_j\rangle| \neq 1$ for some i,j, then one cannot always get the same outcome: a_i in the a setting and b_j in the b setting. In other words, it is impossible to *prepare* [34] a quantum system in a state (in this case, no quantum state exists) that can provide $(\vec{p},\vec{q})$, where $p_i = 1 = q_j$, which identifies an extreme point of Ω.

So, other than (5)–(8), there are certain constraints that are purely quantum mechanical in nature and must be obeyed by $\vec{p}$ and $\vec{q}$ *together*. In our case, QCs are the TIs given in (12), which arise naturally from the structure of the Hilbert space on which quantum theory is based. To write the TIs, we need

$$r_{ij} = |\langle a_i|b_j\rangle|^2 \quad (1 \leqslant i,j \leqslant d), \tag{9}$$

which is the probability of getting outcome a_i if $|b_j\rangle\langle b_j|$ (or b_j if $|a_i\rangle\langle a_i|$) is our state for the system. Like α_i and

β_j in (4),

$$\theta_{ij} = \arccos |\langle a_i|b_j\rangle| \tag{10}$$

is the angle between the pure states $|a_i\rangle\langle a_i|$ and $|b_j\rangle\langle b_j|$. Regarding the subscripts of r_{ij} and θ_{ij}, from left, the first and second indices are reserved for $\mathcal{B}_a$ and $\mathcal{B}_b$, respectively. Therefore, note that $r_{ji} = |\langle a_j|b_i\rangle|^2$ is different from r_{ij}, and likewise for θ.

After choosing the measurement settings, $\mathcal{B}_a$ and $\mathcal{B}_b$ in (1), the entries in

$$R := \begin{pmatrix} r_{11} & \cdots & r_{1d} \\ \vdots & \ddots & \vdots \\ r_{d1} & \cdots & r_{dd} \end{pmatrix} \quad \text{and} \quad \Theta := \begin{pmatrix} \theta_{11} & \cdots & \theta_{1d} \\ \vdots & \ddots & \vdots \\ \theta_{d1} & \cdots & \theta_{dd} \end{pmatrix} \tag{11}$$

get fixed by (9) and (10). All entries in R and in Θ belong to $[0,1]$ and $[0,\frac{\pi}{2}]$, respectively. The sum of all the entries in each row and each column of R is 1, thus it is a doubly stochastic matrix. If the two measurement settings described by (1) are physically the same, then R will be a permutation matrix. For every state vector $|\psi\rangle \in \mathscr{H}_d$, there are three TIs,

$$|\theta_{ij} - \beta_j| \leqslant \alpha_i \leqslant \theta_{ij} + \beta_j, \tag{12}$$

attached to each entry in Θ. These TIs [see (A20)] are derived in Appendix A.

For simplicity, of the three TIs, (12), here we choose only one,

$$\theta_{ij} \leqslant \alpha_i + \beta_j \quad \text{for every} \quad 1 \leqslant i,\ j \leqslant d\,. \tag{13}$$

The angles α_i and β_j vary, whereas θ_{ij} is fixed, as we change the state vector $|\psi\rangle$. The kets that saturate a TI, (13) for certain i,j, lie in the linear span of $\{|a_i\rangle,|b_j\rangle\}$ [consider (A14) and (A15), with $0 \leqslant \beta \leqslant \theta$, from Appendix A]. In the triangle *equality* $\theta_{ij} = \alpha_i + \beta_j$, α_i and β_j are reminiscent of complementary angles from planar geometry, and $0 \leqslant \alpha_i, \beta_j \leqslant \theta_{ij}$. Identifying f, D, and B in [13] by our $|\psi\rangle$, $|a\rangle\langle a|$, and $|b\rangle\langle b|$, respectively, one can see that the TI $\theta \leqslant \alpha + \beta$ is obtained by Landau and Pollak for continuous-time signals (see also Sec. 8 in [14]). They also plotted elliptic curves (for different θs); one of these is shown in Fig. 1, between point E_1 and point E_2 (see also [16]). The results in [13] and [16] are more general than those here, but they are only for a pair of projectors, whereas we take every possible pair $|a_i\rangle\langle a_i|$ and $|b_j\rangle\langle b_j|$ and present three TIs [see (12)], not just one, for each pair.

The cosine function is strictly decreasing in $[0,\pi]$, so applying it to both sides of TI (13) and using (3), (4), (9), and (10), we obtain

$$\sqrt{p_i\, q_j} \leqslant \sqrt{r_{ij}} + \sqrt{(1-p_i)(1-q_j)} \tag{14}$$

after rearrangement of terms. As both sides in (14) are nonnegative functions of the probabilities, squaring and further simplification lead to

$$p_i + q_j \leqslant r_{ij} + 1 + 2\sqrt{r_{ij}(1-p_i)(1-q_j)} \tag{15}$$

for every $1 \leqslant i,\ j \leqslant d$.

All the pairs $(\vec{p},\vec{q}) \in \Omega$ that obey QC (15) for every $1 \leqslant i,\ j \leqslant d$ make up the combined-probability space $\boldsymbol{\omega}$ for the two measurement bases in (1). In the case of $d > 2$, even if we consider all TIs given in (12) for each $1 \leqslant i,\ j \leqslant d$, they do not capture the full QCs for a general pair of settings. Therefore, one can still find some $(\vec{p},\vec{q}) \in \boldsymbol{\omega}$ that corresponds to no quantum state. Nevertheless, our analysis relies on the following fact: *Every* $(\vec{p},\vec{q})$ *that does not belong to* $\boldsymbol{\omega}$ *cannot be obtained from a quantum state, thus it is discarded.* To investigate a space $\boldsymbol{\omega}_{\rm Q}$—which contains all those, and only those, pairs $(\vec{p},\vec{q})$ that originate from quantum states—is not the aim of this paper. However, it is not tough to realize that $\boldsymbol{\omega}_{\rm Q} = \boldsymbol{\omega}$ for $d = 2$; in general, $\boldsymbol{\omega}_{\rm Q} \subseteq \boldsymbol{\omega}$.

Note that $\boldsymbol{\omega}$ is a *proper* subset of Ω. To prove this one can show that only one of the two extreme points—specified by $p_i = 1 = q_j$ and $p_i = 1 = q_l$, where $j \neq l$—of Ω can belong to $\boldsymbol{\omega}$. Recall that if and only if $r_{ij} = 1$, then the point described by $p_i = 1 = q_j$ belongs to $\boldsymbol{\omega}$; otherwise $\theta_{ij} \leqslant \alpha_i + \beta_j$ will be violated. Also, if $r_{ij} = 1$, then $r_{il} = 0$, and $\theta_{il} \leqslant \alpha_i + \beta_l$ cannot be obeyed by the other point; hence that stays outside of $\boldsymbol{\omega}$.

The space $\boldsymbol{\omega}$ is—held by conditions (5)–(8) and (15)—a compact and convex subset of $\mathbb{R}^{2d}$ (for a proof, see Appendix B). Every point in such a set can be written as a convex combination of its extreme points due to the Krein-Milman theorem (see Theorem 3.3.5 and Appendix A.3 in [15]). We begin our journey from an interior point in $\boldsymbol{\omega}$ in Appendix D 1 and arrive at its extreme points at the end of Appendix D 3. There it is concluded that the set of all extreme points of $\boldsymbol{\omega}$ comes from a family of parametric curves.

One can skip all those technical details and start constructing the parametric curves straight from the conclusion, (D56): the first step is to pick a set of m angles from a single column or row in matrix Θ given in (11). This is called the m set, and $1 \leqslant m \leqslant d-1$. For instance, we pick the top m angles $\{\theta_{i1}\}_{i=1}^{m}$ from the first column. Then we associate m triangular equalities with the m set as

$$\alpha_i = \theta_{i1} - \beta_1 \quad \text{for all} \quad i = 1,\ldots,m \tag{16}$$

by taking β_1, where the subscript 1 reflects the selected column.

Next, with (3) and (4), we assign $m+1$ probabilities to the angles: $p_i = (\cos\alpha_i)^2$ and $q_1 = (\cos\beta_1)^2$. They create the probability vectors

$$\vec{p}_{(\beta_1)} = ((\cos\alpha_1)^2,\ldots,(\cos\alpha_m)^2,\mathbf{0},\, p_s,\mathbf{0}), \tag{17}$$

$$\vec{q}_{(\beta_1)} = ((\cos\beta_1)^2,\mathbf{0},q_t,\mathbf{0}), \tag{18}$$

where

$$p_s = 1 - \sum_{i=1}^{m}(\cos\alpha_i)^2 \quad (m+1 \leqslant s \leqslant d), \tag{19}$$

$$q_t = 1 - (\cos\beta_1)^2 \quad (2 \leqslant t \leqslant d), \quad \text{and} \tag{20}$$

$$\mathbf{0} \equiv 0,\ldots,0. \tag{21}$$

One can observe that $(\vec{p}_{(\beta_1)}, \vec{q}_{(\beta_1)})$ serves as a vector-valued function of a single real parameter β_1, thus it exhibits a parametric curve. Since the curve is associated with an m set and all its points obey m triangle equalities, (16), we call it an m-parametric curve.

A part of the curve, identified by the upper and lower limits $\beta' \leqslant \beta_1 \leqslant \beta''$, lies in $\boldsymbol{\omega}$ and represents its extreme points because $(\vec{p}_{(\beta_1)}, \vec{q}_{(\beta_1)})$ cannot be written into a convex combination of other points of $\boldsymbol{\omega}$. In Appendix D 4, we realize that the two limits are fixed by

$$p_{s(\beta')} = [\cos(\theta_{s1} - \beta')]^2 \quad \text{when} \quad 1 \leqslant m \leqslant d-1, \tag{22}$$

$$\beta'' = \frac{\theta_{11} - \theta_{1t}}{2} + \frac{\pi}{4} \quad \text{when} \quad 1 = m, \quad \text{and} \tag{23}$$

$$p_{s(\beta'')} = 0 \quad \text{when} \quad 1 < m \leqslant d-1 \tag{24}$$

[see (D74)]. Equations (22) and (24) are like Eq. (D73), whose roots are stated in (D80). Always the root with a positive sign delivers the correct limit (for justifications, see the last paragraph in Appendix D 4).

If one chooses an m set from a row of Θ, say $\{\theta_{1j}\}_{j=1}^{m}$, then the m-parametric curve is constructed as

$$\beta_j = \theta_{1j} - \alpha_1 \quad \text{for all} \quad j = 1, \ldots, m, \tag{25}$$

$$\vec{p}_{(\alpha_1)} = ((\cos\alpha_1)^2, \mathbf{0}, p_s, \mathbf{0}), \tag{26}$$

$$\vec{q}_{(\alpha_1)} = ((\cos\beta_1)^2, \ldots, (\cos\beta_m)^2, \mathbf{0}, q_t, \mathbf{0}), \tag{27}$$

$$p_s = 1 - (\cos\alpha_1)^2 \quad (2 \leqslant s \leqslant d), \quad \text{and} \tag{28}$$

$$q_t = 1 - \sum_{j=1}^{m} (\cos\beta_j)^2 \quad (m+1 \leqslant t \leqslant d). \tag{29}$$

Now the parameter is $\alpha_1 \in [\alpha', \alpha'']$, and the limits are determined by

$$q_{t(\alpha')} = [\cos(\theta_{1t} - \alpha')]^2 \quad \text{when} \quad 1 \leqslant m \leqslant d-1, \tag{30}$$

$$\alpha'' = \frac{\theta_{11} - \theta_{s1}}{2} + \frac{\pi}{4} \quad \text{when} \quad 1 = m, \quad \text{and} \tag{31}$$

$$q_{t(\alpha'')} = 0 \quad \text{when} \quad 1 < m \leqslant d-1. \tag{32}$$

One can check that, for $m = 1$, both (16)–(23) and (25)–(31) describe the same thing, provided s and t are identical in both cases. So an m-parametric curve is identified by an m set and the positions of p_s and q_t (that is, s and t) in $\vec{p}$ and $\vec{q}$, respectively.

Let us count the total number of curves described by (16)–(20). One can harvest $\frac{d!}{m!(d-m)!}$ distinct m sets from a single column in Θ, and there are d total columns. The probability p_s can take $d-m$ different places in $\vec{p}$ of (17) for distinct s, and q_t can take $d-1$ different places in $\vec{q}$ of (18) for distinct t. Thus we have $(d-m)(d-1)$ individual m-parametric curves with a single m set. Since $1 \leqslant m \leqslant d-1$, we collect the number of curves

$$d \sum_{m=1}^{d-1} \frac{d!}{m!(d-m)!}(d-1)(d-m), \tag{33}$$

where each m set is made up of angles from a column in Θ.

We secure the same number if we consider rows, rather than columns, to construct an m set and then a curve such as given by (25)–(29). For $m = 1$, every m set appears in a row as well as in a column. So, to avoid double-counting errors, we take the cases $m = 1$ and $m > 1$ separately. In total, the number of parametric curves for a qudit is

$$d^2(d-1)^2 + 2d \sum_{m=2}^{d-1} \frac{d!}{m!(d-m)!}(d-1)(d-m)$$
$$= d^2(d-1)[2^d - (d+1)]. \tag{34}$$

If one adopts a suitable concave function $\mathsf{u}(\vec{p},\vec{q})$ on the combined space $\boldsymbol{\omega}$ to estimate the uncertainty, then its absolute minimum will occur *only* at the parametric curves (see Theorem 3.4.7 and Appendix A.3 in [15]). So ultimately one needs to find absolute minima of, at most, $d^2(d-1)[2^d - (d+1)]$ functions, each of a single variable [for example, see (42)]. Then the smallest minimum will be the lower bound $\mathsf{c} \leqslant \mathsf{u}$ in a UR. This task can be easily completed on a regular computer. In the next two sections, we discuss certain concave as well as convex functions on $\boldsymbol{\omega}$.

III. UNCERTAINTY MEASURES AND RELATIONS

If u quantifies the uncertainty—about the outcomes a_i when a qudit is measured in the basis $\mathcal{B}_a$ of (1)—then u should be a concave function of $\vec{p} \in \Omega_a$. This is because the mixing probability distributions, $\vec{p}\,'$ and $\vec{p}\,''$ as $\lambda\,\vec{p}\,' + (1-\lambda)\vec{p}\,'' = \vec{p}$ with $\lambda \in [0,1]$, can only increase the uncertainty $\lambda\,u(\vec{p}\,') + (1-\lambda)u(\vec{p}\,'') \leqslant u(\vec{p})$ (see Chap. 9 in [33]). In this regard, every mixed state, say $\lambda|\psi'\rangle\langle\psi'| + (1-\lambda)|\psi''\rangle\langle\psi''| = \rho_{\text{mix}}$, has greater uncertainty.

So, here, we adopt a real-valued smooth concave function,

$$u(\vec{p}) := \sum_{i=1}^{d} \sqrt{p_i}, \tag{35}$$

as an uncertainty measure. It is associated with the Tsallis entropy [35], $S_{1/2}(\vec{p}) = 2K(u(\vec{p}) - 1)$, where K is the Boltzmann constant. To prove that $u(\vec{p})$ is a concave function on Ω_a, it is sufficient to demonstrate that the $(d-1) \times (d-1)$ Hessian matrix—which is a symmetric matrix of second-order partial derivatives of u—is a negative semidefinite matrix at every point in Ω_a (see Theorem 4.5 in [36]). At an interior point (where all $p_i > 0$) of Ω_a, the entry in the kth row and lth column $(1 \leqslant l, k \leqslant d-1)$ in the Hessian matrix is

$$\frac{\partial^2 u}{\partial p_k \partial p_l} = -\frac{1}{4}\left(\frac{1}{p_l^{3/2}}\delta_{lk} + \frac{1}{p_d^{3/2}}\right) = \frac{\partial^2 u}{\partial p_l \partial p_k}, \tag{36}$$

where $p_d = 1 - \sum_{i=1}^{d-1} p_i$ and δ_{lk} is the Kronecker delta function. These entries indeed provide a negative definite matrix, thus $u(\vec{p})$ is strictly concave in the interior of Ω_a. At a boundary point (where one or more $p_i = 0$), all the partial derivatives in a certain row(s) and column(s) of the Hessian matrix become 0, thus the matrix turns out to be a negative semidefinite and $u(\vec{p})$ to be a concave function. By the way, $u(\vec{p})$ can be employed for entanglement detection (see Remark 3 in [37]).

If the state vector $|\psi\rangle$ is an equal superposition of all the kets in $\mathcal{B}_a$ or the state is completely mixed, then all the outcomes a_i will be equally probable: $p_i = \frac{1}{d}$ for every $1 \leqslant i \leqslant d$ is the center of Ω_a, where $u(\vec{p})$ reaches its maximum value $\sqrt{d}$. However, only in the case of a definite outcome—that is, when $|\psi\rangle\langle\psi| = |a_i\rangle\langle a_i|$ and then $p_i = 1$ for a particular i—we have

the minimum uncertainty $u(\vec{p}) = 1$ as it should be. Note that $p_i = 1$ characterizes an extreme point in Ω_a.

To establish a measure of combined uncertainty for the experimental proposal, (2), we take the same function,

$$u(\vec{q}) = \sum_{j=1}^{d} \sqrt{q_j}, \tag{37}$$

for the b setting. Like $u(\vec{p})$ of (35), $u(\vec{q})$ is a concave function on Ω_b with the range $[1, \sqrt{d}\,]$. Now we define our combined uncertainty measure

$$\mathfrak{u}(\vec{p},\vec{q}) := u(\vec{p}) + u(\vec{q}) = \sum_{l=1}^{d} (\sqrt{p_l} + \sqrt{q_l}) \tag{38}$$

on the convex set $\boldsymbol{\omega}$, rather than Ω. The sum of two concave functions is concave, so $\mathfrak{u}$ is also a concave function.

A mixed quantum state is a convex combination of pure states, the probabilities

$$p_i = \mathrm{tr}(\varrho\, |a_i\rangle\langle a_i|) \quad \text{and} \quad q_j = \mathrm{tr}(\varrho\, |b_j\rangle\langle b_j|) \tag{39}$$

are linear functions of the state ϱ [$0 \leqslant \varrho$, $\mathrm{tr}(\varrho) = 1$], and $\boldsymbol{\omega}$ is a compact and convex set. As a result, every $(\vec{p},\vec{q})$ associated with any (pure or mixed) quantum state lies in $\boldsymbol{\omega}$. And because $\mathfrak{u}$ is a concave function on $\boldsymbol{\omega}$, our UR given in (40) applies to every state for a qudit. This is also true in the case of other certainty and uncertainty relations presented in Sec. IV, because there also we mostly have either a concave or a convex function. In (93) and (94), the functions are neither concave nor convex on $\boldsymbol{\omega}$, but the relations are followed by every qubit's state. By the way, one can check that if $\varrho = |\psi\rangle\langle\psi|$, then the Born rule, (39), reduces to (3).

The range of $\mathfrak{u}(\vec{p},\vec{q})$ and our UR is presented as

$$2 \leqslant \mathfrak{c} \leqslant \mathfrak{u}(\vec{p},\vec{q}) \leqslant 2\sqrt{d}, \tag{40}$$

where

$$\mathfrak{c} := \min_{(\vec{p},\vec{q}) \in \boldsymbol{\omega}} \mathfrak{u}(\vec{p},\vec{q}) \tag{41}$$

is the global minimum, which will occur on the m-parametric curves (given in Sec. II). However, $\mathfrak{u}$ gains its absolute maximum $2\sqrt{d}$ only at the point identified by $p_i = \frac{1}{d} = q_j$ for all $1 \leqslant i,\ j \leqslant d$. This is called the *center* of $\boldsymbol{\omega}$, which represents a uniform distribution for both settings. Now recall from Sec. II that an extreme point in Ω, described by $p_i = 1 = q_j$, belongs to $\boldsymbol{\omega}$ if and only if $|a_i\rangle\langle a_i| = |b_j\rangle\langle b_j|$. Only in such a situation—which does not necessarily require both bases, $\mathcal{B}_a$ and $\mathcal{B}_b$, to be the same in any way—we have the *trivial* lower bound $\mathfrak{c} = 2$ and thus the UR $2 \leqslant \mathfrak{u}$. A similar statement is made by Deutsch in [6]. For $d = 2$, the trivial case is possible if and only if the two measurement settings are (physically) the same. A nontrivial lower bound $\mathfrak{c} > 2$ materializes when the settings are completely different, that is, when $r_{ij} < 1$ for every $1 \leqslant i,\ j \leqslant d$. So the following analysis is obviously for nontrivial cases.

To find the lower bound, (41), and to establish the UR $\mathfrak{c} \leqslant \mathfrak{u}$, we write the functional form

$$\mathfrak{u}(\beta_1) = \sum_{i=1}^{m} \cos\alpha_i + \sqrt{p_s} + \cos\beta_1 + \sin\beta_1, \tag{42}$$

which $\mathfrak{u}(\vec{p},\vec{q})$ of (38) acquires on an m-parametric curve specified by (16)–(21). To show that $\mathfrak{u}$ of (42) is a concave function of β_1, we present

$$\frac{\partial^2 \mathfrak{u}}{\partial {\beta_1}^2} = -\left[\sum_{i=1}^{m} \cos\alpha_i + \cos\beta_1 + \sin\beta_1\right] + \frac{\partial^2 \sqrt{p_s}}{\partial {\beta_1}^2}, \tag{43}$$

$$\frac{\partial^2 \sqrt{p_s}}{\partial {\beta_1}^2} = -\frac{1}{4\, {p_s}^{3/2}} \left(\frac{\partial p_s}{\partial \beta_1}\right)^2 + \frac{1}{2\sqrt{p_s}} \frac{\partial^2 p_s}{\partial {\beta_1}^2}, \quad \text{and} \tag{44}$$

$$\frac{\partial^2 p_s}{\partial {\beta_1}^2} = -2[2\, p_s + (m-2)]. \tag{45}$$

With these derivatives, one can clearly see that $\frac{\partial^2 \mathfrak{u}}{\partial {\beta_1}^2} < 0$ for $1 < m \leqslant d-1$, whereas $\frac{\partial^2 \mathfrak{u}}{\partial {\beta_1}^2} = -\mathfrak{u} < 0$ for $m = 1$. This proves that $\mathfrak{u}$ is a (strictly) concave function on every parametric curve. Therefore, its global minimum $\mathfrak{c}$ will always be at the endpoints of the curves. The endpoints of an m-parametric curve are identified by the two limits on a parameter [see (22)–(24) as well as (30)–(32)].

It is shown in Appendix D 4 that, to compute a limit, we always have to solve an equation such as (D73), which carries M number of angles from a column or a row in Θ [given in (11)]. Note that we use the lowercase letter m ($1 \leqslant m \leqslant d-1$) when we construct a parametric curve with an m set (see Sec. II) and use a small-capital letter M ($2 \leqslant \mathrm{M} \leqslant d$) when we compute a limit with an M set. Essentially, one needs to follow a three-step procedure to compute a limit and then the value of $\mathfrak{u}$ [defined in (38); see also (42)] at the corresponding endpoint of a curve:

1. Pick an M set from a column or a row in Θ, say $\{\theta_1, \ldots, \theta_{\mathrm{M}}\}$; here only one index of θ is shown.

2. Solve $\sum_{l=1}^{\mathrm{M}} [\cos(\theta_l - \chi)]^2 = 1$ for χ,

which represents a limit.

3. Compute $c_{\mathrm{M}} := \sum_{l=1}^{\mathrm{M}} \cos(\theta_l - \chi) + \cos\chi + \sin\chi$,

which is the value of $\mathfrak{u}$ at an endpoint. (46)

The equation in step 2 is like Eq. (D73), which is solved in Appendix D 4, and every time we take the solution (D80) with the positive sign. One can observe that χ and therefore c_{M} are determined solely by the M set picked in step 1.

After repeating the three-step procedure for every M set and for each $2 \leqslant \mathrm{M} \leqslant d$, we collect a set of values $\{c_{\mathrm{M}}\}$ for all the endpoints. Then the smallest value in this set will be $\mathfrak{c}$ [defined by (41)], and thus we have our UR $\mathfrak{c} \leqslant \mathfrak{u}$ [presented in (40)]. Since every c_{M} is determined by the entries in the Θ matrix, the lower bound $\mathfrak{c}$ depends only on the measurement bases in (1), and is *independent* of the quantum state. Besides, to compute $\mathfrak{c}$, we can employ an ordinary computer, which repeats the

three steps in (46) by taking one by one the number of M sets

$$2d\sum_{\mathrm{M}=2}^{d}\frac{d!}{\mathrm{M}!(d-\mathrm{M})!}=2d\,[2^d-(d+1)]. \tag{47}$$

In fact, $2d\,[2^d-(d+1)]$ is the total number of endpoints for a qudit.

Although we have the solution, (D80), for step 2, it is easy to calculate χ and c_{M} for $\mathrm{M}=2,d$. For a two-set $\{\theta_1,\theta_2\}$, one can directly realize

$$\chi=\frac{\theta_1+\theta_2}{2}-\frac{\pi}{4}, \tag{48}$$

and then

$$c_2(\theta_1,\theta_2)=\sqrt{2}\left[\cos\left(\frac{\theta_1-\theta_2}{2}\right)+\sin\left(\frac{\theta_1+\theta_2}{2}\right)\right] \tag{49}$$

$$=\frac{1}{\sqrt{2}}\left(\sqrt{1+\sqrt{r_1}}+\sqrt{1-\sqrt{r_1}}\right)\left(\sqrt{1+\sqrt{r_2}}+\sqrt{1-\sqrt{r_2}}\right). \tag{50}$$

Every endpoint of an $m=1$ parametric curve is determined by a set of $\mathrm{M}=2$ angles [see (22), (23), (30), and (31)]. For a d set $\{\theta_1,\ldots,\theta_d\}$, that is, an entire column or row of Θ, we have the total probability $\sum_{l=1}^{d}(\cos\theta_l)^2=1$. Therefore, we obtain the solution

$$\chi=0, \tag{51}$$

and then

$$c_d(\theta_1,\ldots,\theta_d)=\sum_{l=1}^{d}\cos\theta_l+1=\sum_{l=1}^{d}\sqrt{r_l}+1. \tag{52}$$

For general measurement settings, it is easy to compute, but difficult to express $\mathfrak{c}$, in an analytic form. Nevertheless, we present it for $d=2,3$, and when the measurement bases in (1) are MUBs [19].

In the case of a qubit, $d=2$, a certainty or uncertainty relation can be stated with the three probabilities p_1, q_1, and r_{11}, hence we drop the subscripts here and in the next section. Furthermore, all the TIs, (13), can now be put together as

$$\theta\leqslant\alpha+\beta\leqslant\pi-\theta\quad\text{and}\quad|\alpha-\beta|\leqslant\theta, \tag{53}$$

where α, β, and θ are associated with p, q, and r, respectively [through (3), (4), (9), and (10)]. Here only $m=1$ parametric curves exist, which are total four [see with (34)]. To draw the endpoint of a curve, we can use either (48) or (51); both are equal (because $\theta_1+\theta_2=\frac{\pi}{2}$). There are only four [see (47)] endpoints, $E_1,\ldots,E_4$. Next, one can realize that (49) and (52) are also the same for a qubit. Furthermore, c_d is even identical for every $\mathrm{M}=2$ set. This implies that our combined uncertainty function, (38), takes the same value at all four endpoints, thus $\mathfrak{c}=c_d=c_2$ and

$$\underbrace{\sqrt{r}+\sqrt{1-r}+1}_{\mathfrak{c}(r)}\leqslant\underbrace{\sqrt{p}+\sqrt{1-p}+\sqrt{q}+\sqrt{1-q}}_{\mathfrak{u}(p,q)} \tag{54}$$

is a UR for $d=2$. This is also given in [25].

Together all the parametric curves—which represent all the extreme points of the combined-probability space $\boldsymbol{\omega}$—can be

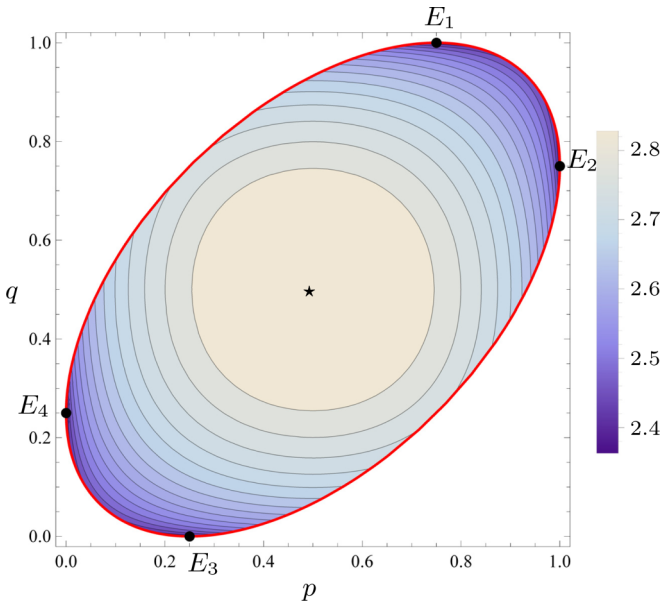

FIG. 1. Contour plot of $\mathfrak{u}(p,q)$ on $\boldsymbol{\omega}$ for $d=2$ and $r=\frac{3}{4}$, where a darker shade represents a smaller value of $\mathfrak{u}$. Square-shaped and elliptical regions represent Ω and $\boldsymbol{\omega}$, respectively. Note that $\boldsymbol{\omega}\subset\Omega\subset\mathbb{R}^4$ and the unseen coordinates are $p_2=1-p$ and $q_2=1-q$ for each point. For every $r\in[0,1]$, $\mathfrak{u}$ hits its global minimum $\mathfrak{c}$ [given in (54)] on $\boldsymbol{\omega}$ at all four points $E_1,\ldots,E_4$, which are shown by small black circles. And $\mathfrak{u}$ always achieves its global maximum $2\sqrt{2}$ [stated in (40)] at the center, $p=\frac{1}{2}=q$, indicated by the black star, of $\boldsymbol{\omega}$.

expressed by an ellipse,

$$(p_{(\vartheta)},q_{(\vartheta)})=([\cos(\theta-\vartheta)]^2,(\cos\vartheta)^2)\quad\text{with}\quad\vartheta\in[0,\pi), \tag{55}$$

in the case of a qubit. As a special case, the same ellipse also appears in [16–18] through different routes [38], although our approach is closer to that in [16]. One can observe that the ellipse becomes a circle for $\theta=\frac{\pi}{4}$ and becomes certain line segments for $\theta=0,\frac{\pi}{2}$. In Fig. 1, we present a contour plot of $\mathfrak{u}(p,q)$ on $\boldsymbol{\omega}$ by taking $r=\frac{3}{4}$. So $\theta=\frac{\pi}{6}$, and one can see that $\boldsymbol{\omega}$ is bounded by the ellipse, (55). Furthermore, by putting $\vartheta=0$, θ, $\frac{\pi}{2}$, and $\frac{\pi}{2}+\theta$ in $(p_{(\vartheta)},q_{(\vartheta)})$, we can have the four endpoints E_1, E_2, E_3, and E_4, respectively.

In the case of $d=2$, there always exists a quantum state for each point in $\boldsymbol{\omega}$, thus $\boldsymbol{\omega}=\boldsymbol{\omega}_{\mathrm{Q}}$. For instance, kets such as (A14) and (A15) correspond to points on the ellipse, (55), by the Born rule, (3). In particular, the kets of basis $\mathcal{B}_a$ correspond to the points $\{E_2,E_4\}$, and the kets of $\mathcal{B}_b$ are related to $\{E_1,E_3\}$. So the lower bound $\mathfrak{c}(r)$ in the UR, (54), is achieved—hence, it is a *tight* UR—only by those state vectors $|\psi\rangle$ that (up to a phase factor) belong to one of the bases in (1). The lower bound will be the largest, $\sqrt{2}+1$, when $r=\frac{1}{2}$, that is, the measurement bases are MUBs [see also (58)].

A UR is called tight if there exists a quantum state that saturates it. In the case of the qubit, all the relations mentioned in this and the next section are tight because $\boldsymbol{\omega}=\boldsymbol{\omega}_{\mathrm{Q}}$. For $d\geqslant 3$, $\boldsymbol{\omega}_{\mathrm{Q}}\subseteq\boldsymbol{\omega}$, hence our UR $\mathfrak{c}\leqslant\mathfrak{u}$ is not tight in general.

In the case of $d = 3$ (a qutrit), there are only two kinds of parametric curves (for $m = 1,2$), and two types of endpoints (for $\mathrm{M} = 2,3$). So (48) and (51) can specify any endpoint for a qutrit. To compute the lower bound $\mathfrak{c}$, we have to evaluate the functions c_2 of (49) for every two-set and c_d of (52) every d set drawn from the Θ matrix. For $d = 3$, there are 18 two-sets and 6 d sets [see the total in (47)]. Then the smallest of the $18 + 6 = 24$ values will be our $\mathfrak{c}$. Now let us consider a pair of MUBs [19] for a finite dimension d.

If the two bases given in (1) are such that $r_{ij} = \frac{1}{d}$ for every $1 \leqslant i, j \leqslant d$ [for r_{ij}, see (9)], then they are called MUBs and the measurement settings a and b are designated *complementary* [7]. In the case of MUBs, $\theta_{ij} = \arccos \frac{1}{\sqrt{d}}$ for every i, j, so one can straightforwardly realize

$$\chi = \arccos \frac{1}{\sqrt{d}} - \arccos \frac{1}{\sqrt{\mathrm{M}}}, \quad \text{and} \tag{56}$$

$$c_{\mathrm{M}} = \sqrt{\mathrm{M}} + \frac{1 + \sqrt{(d-1)(\mathrm{M}-1)} + \sqrt{d-1} - \sqrt{\mathrm{M}-1}}{\sqrt{d\,\mathrm{M}}} \tag{57}$$

in steps 2 and 3 of the three-step procedure, (46). One can acknowledge that here χ and c_{M} depend on $\mathrm{M} = 2, \ldots, d$, not on a particular M set, because every θ is the same. Furthermore, χ decreases, whereas c_{M} increases, with M. Hence the lower bound is

$$\mathfrak{c}_{\mathrm{MUB}}^{(d)} = c_2 = \sqrt{2}\left(1 + \frac{\sqrt{d-1}}{\sqrt{d}}\right), \tag{58}$$

which does not deliver a tight UR when $d > 2$, whereas tight URs [7,8,22] are known for MUBs in a finite d. We close this section with the following remarks.

Remark 1. By the Born rule, (3), $|\psi\rangle = |a_i\rangle$ provides an extreme point, given by $p_i = 1$ and $\vec{q} = (r_{i1}, \ldots, r_{id})$, of $\boldsymbol{\omega}$ [see (D33) and (D32) in Appendix D 3]. At this point the combined uncertainty function, (38), has the value $1 + \sum_{j=1}^{d} \sqrt{r_{ij}}$ [see also (52)]. Likewise, $|\psi\rangle = |b_j\rangle$ gives the combined uncertainty $1 + \sum_{i=1}^{d} \sqrt{r_{ij}}$. Now we take the minimum value

$$\mathfrak{c}_{\mathrm{bases}} := \min\{\mathfrak{u}_a, \mathfrak{u}_b\}, \tag{59}$$

where

$$\mathfrak{u}_a := \min_{1 \leqslant i \leqslant d} \left\{1 + \sum_{j=1}^{d} \sqrt{r_{ij}}\right\} \quad \text{and} \tag{60}$$

$$\mathfrak{u}_b := \min_{1 \leqslant j \leqslant d} \left\{1 + \sum_{i=1}^{d} \sqrt{r_{ij}}\right\}. \tag{61}$$

Next, one can easily establish

$$2 \leqslant \mathfrak{c} \leqslant \mathfrak{c}_{\mathrm{Q}} \leqslant \mathfrak{c}_{\mathrm{bases}} \leqslant 1 + \sqrt{d}, \tag{62}$$

where

$$\mathfrak{c}_{\mathrm{Q}} := \min_{|\psi\rangle \in \mathscr{H}_d} \mathfrak{u}(\vec{p}, \vec{q}). \tag{63}$$

The first inequality in (62) comes from (40). The last inequality is due to $\sum_{i=1}^{d} \sqrt{r_{ij}} \leqslant \sqrt{d}$ and the same relation where the summation is over index j instead of i. $\mathfrak{c}_{\mathrm{Q}}$ is the *largest* lower bound, which defines the *tight* UR $\mathfrak{c}_{\mathrm{Q}} \leqslant \mathfrak{u}(\vec{p}, \vec{q})$. For $d = 2$, our lower bound $\mathfrak{c} = \mathfrak{c}_{\mathrm{Q}} = \mathfrak{c}_{\mathrm{bases}}$, and the UR, (54), is tight. However, if the two bases in (1) share a ket, then $\mathfrak{c}$ turns out to be the trivial bound: $2 = \mathfrak{c} = \mathfrak{c}_{\mathrm{Q}} = \mathfrak{c}_{\mathrm{bases}}$. One can use (62) to avoid errors when calculating $\mathfrak{c}$.

Remark 2. The function $H_{1/2}(\vec{p}) = 2 \ln u(\vec{p})$ is the Rényi entropy [39] of order $\frac{1}{2}$. Using (36), one can realize that $H_{1/2}(\vec{p})$ is a concave function on Ω_a, hence the sum

$$H_{1/2}(\vec{p}) + H_{1/2}(\vec{q}) = 2 \ln[u(\vec{p})u(\vec{q})] \tag{64}$$

is concave on $\boldsymbol{\omega}$. Taking (43)–(45), one can confirm that the sum is also concave on each of the parametric curves, therefore its absolute minimum will be at the endpoints. By repeating the three-step procedure, (46)—where in the third step now we need to compute

$$h_{\mathrm{M}} := 2 \ln \left\{\left[\sum_{l=1}^{\mathrm{M}} \cos(\theta_l - \chi)\right](\cos\chi + \sin\chi)\right\} \tag{65}$$

instead of c_{M}—for every M set, we can obtain a UR based on the combined entropy, (64), for any pair of measurement settings. Analogous to (49), (52), and (57), here we have

$$\begin{aligned} h_2(\theta_1, \theta_2) &= 2 \ln \left[2 \cos\left(\frac{\theta_1 - \theta_2}{2}\right) \sin\left(\frac{\theta_1 + \theta_2}{2}\right)\right] \\ &= 2 \ln \left[\sqrt{1 - r_1} + \sqrt{1 - r_2}\right], \end{aligned} \tag{66}$$

$$h_d(\theta_1, \ldots, \theta_d) = 2 \ln \sum_{l=1}^{d} \cos\theta_l = 2 \ln \sum_{l=1}^{d} \sqrt{r_l}, \quad \text{and} \tag{67}$$

$$h_{\mathrm{M}} = 2 \ln \left[\frac{1 + \sqrt{(d-1)(\mathrm{M}-1)} + \sqrt{d-1} - \sqrt{\mathrm{M}-1}}{\sqrt{d}}\right], \tag{68}$$

respectively; with these one can directly get URs for a qubit, a qutrit, and a pair of MUBs just like above. For a qubit, we express the corresponding tight UR (also obtained in [25])

$$\sqrt{r} + \sqrt{1 - r} \leqslant \left(\sqrt{p} + \sqrt{1 - p}\right)\left(\sqrt{q} + \sqrt{1 - q}\right) \tag{69}$$

in terms of the product $u(p)u(q)$. In this case, the product turns out to be a concave function not only on $\boldsymbol{\omega}$ but also on each of the four parametric curves. And its absolute minimum—given on the left-hand side of (69)—occurs at all four endpoints $E_1, \ldots, E_4$, and the absolute maximum 2 at the center (denoted by the black star in Fig. 1) of $\boldsymbol{\omega}$.

IV. OTHER CERTAINTY AND UNCERTAINTY MEASURES AND RELATIONS

The negative of a concave function is a convex function, hence a suitable convex function can be taken as a measure of certainty, rather than uncertainty. Here we present other popular measures of certainty and uncertainty and obtain the associated certainty and uncertainty relations for $d = 2$ by finding the absolute maximum (for convex) and minimum (for concave) on the ellipse, (55). We want to emphasize that all the relations given in this paper for a qubit are already

known (thanks to [6,8,17] and [25–32]), obtained by different methods. The following analysis merely shows that they all can be obtained from the TIs, (53), that characterize the ellipse. Recall that one can have the same ellipse from [16–18].

One can always construct Hermitian operators, for example,

$$A = \sum_{i=1}^{d} a_i |a_i\rangle\langle a_i| \quad \text{and} \quad B = \sum_{j=1}^{d} b_j |b_j\rangle\langle b_j|, \tag{70}$$

by assigning real numbers to the measurement outcomes a_i and b_j for the two settings specified by (1). Then $\mathbf{a} := \{a_i\}_{i=1}^{d}$ and $\mathbf{b} := \{b_j\}_{j=1}^{d}$ are the sets of eigenvalues of A and B, respectively. With (3) and (70), one can perceive that the squared standard deviations

$$\begin{aligned}\Delta(A,\rho)^2 &= \langle\psi|A^2|\psi\rangle - \langle\psi|A\,|\psi\rangle^2 \\ &= \sum_{i=1}^{d} {a_i}^2\, p_i - \left(\sum_{i=1}^{d} a_i\, p_i\right)^2 = \Delta(\mathbf{a},\vec{p})^2, \end{aligned} \tag{71}$$

$$\Delta(B,\rho)^2 = \sum_{j=1}^{d} {b_j}^2\, q_j - \left(\sum_{j=1}^{d} b_j\, q_j\right)^2 = \Delta(\mathbf{b},\vec{q})^2 \tag{72}$$

are functions of the probabilities as well as the eigenvalues.

Taking $p_d = 1 - \sum_{i=1}^{d-1} p_i$, like the derivatives, (36), of $u(\vec{p})$, we get the second-order partial derivatives

$$\frac{\partial^2\,\Delta^2}{\partial p_k \partial p_l} = -2(a_k - a_d)(a_l - a_d) = \frac{\partial^2\,\Delta^2}{\partial p_l \partial p_k} \tag{73}$$

of function (71) for $1 \leqslant k, l \leqslant d-1$. One can validate that the Hessian matrix—made up of the derivatives, (73)—is a negative semidefinite matrix for any set $\mathbf{a}$ of eigenvalues. Thus, $\Delta(\mathbf{a},\vec{p})^2$ is a concave function on Ω_a (see Theorem 4.5 in [36]). Likewise, $\Delta(\mathbf{b},\vec{q})^2$ is a concave function on Ω_b. Hence, analogous to $u(\vec{p},\vec{q})$ of (38), the sum

$$\boldsymbol{\Delta}^{\text{sq}}(\mathbf{a},\vec{p},\mathbf{b},\vec{q}) := \Delta(\mathbf{a},\vec{p})^2 + \Delta(\mathbf{b},\vec{q})^2 \tag{74}$$

establishes a concave, thus uncertainty, measure on the combined space $\boldsymbol{\omega}$. In [40], URs are presented by taking a sum such as (74), however, here the approach is different.

In the case of a qubit ($d = 2$), every measurement setting can also be described by a three-component real vector. So, we designate the two settings [see (1)] by certain unit vectors, $\widehat{a}$ and $\widehat{b}$, and then construct the Hermitian operators, $A = \widehat{a}\cdot\vec{\sigma}$ and $B = \widehat{b}\cdot\vec{\sigma}$, with the dot product, where $\vec{\sigma}$ is the Pauli vector operator. One can verify that $A^2 = I = B^2$, therefore the eigenvalues are $\mathbf{a} = \{\pm 1\} = \mathbf{b}$. Suppose the kets $|a_1\rangle$ and $|b_1\rangle$ of the two bases [in (1)] are associated with the eigenvalue $+1$ of A and B, respectively. Now one can easily derive the relation

$$\text{tr}(A^\dagger B) = 4\,|\langle a_1|b_1\rangle|^2 - 2 = 2\,\widehat{a}\cdot\widehat{b} \tag{75}$$

between the three kinds of inner products. From Sec. III, let us recall that we only require three probabilities, p_1, q_1, and r_{11}, to express a certainty or uncertainty relation for $d = 2$. So, there is no further need for the subscripts. With all the above considerations, $\boldsymbol{\Delta}^{\text{sq}}$ of (74) turns out to be the function

$$\boldsymbol{\Delta}^{\text{sq}}(\pm 1,p,\pm 1,q) = 1 - (2p-1)^2 + 1 - (2q-1)^2 \tag{76}$$

of p and q.

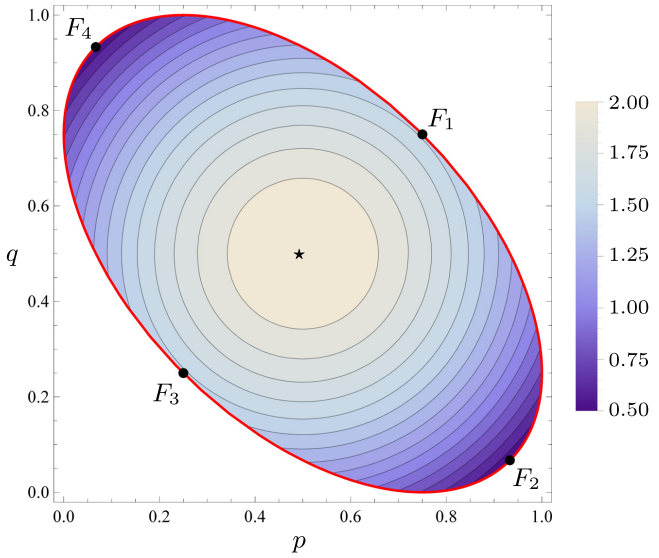

FIG. 2. Contour plot of $\boldsymbol{\Delta}^{\text{sq}}(p,q)$ of (76) on $\boldsymbol{\omega}$, where a darker shade illustrates a smaller value of $\boldsymbol{\Delta}^{\text{sq}}$. Here $r = \frac{1}{4}$, therefore $\boldsymbol{\Delta}^{\text{sq}}$ reaches its global minimum $2r$ [see the UR, (77) and (78)] at the two points F_2 and F_4. However, $\boldsymbol{\Delta}^{\text{sq}}$ always gains its global maximum 2 at the center, $p = \frac{1}{2} = q$, denoted by the black star, of $\boldsymbol{\omega}$. As in Fig. 1, $\boldsymbol{\omega}$ is the region bounded by the ellipse, (55), but $\theta = \frac{\pi}{3}$ here.

We plot $\boldsymbol{\Delta}^{\text{sq}}$ of (76) on $\boldsymbol{\omega}$ in Fig. 2 by taking $r = \frac{1}{4}$. Since $\boldsymbol{\Delta}^{\text{sq}}$ is a concave function on $\boldsymbol{\omega}$, its absolute minimum will be on the four parametric curves, which are jointly described by the ellipse, (55), and by their endpoints, $E_1, \ldots, E_4$. To compute the minimum, first, we need to represent $\boldsymbol{\Delta}^{\text{sq}}$ as a function of a parameter, like u in (42), on each curve. Then we have to find the critical points of $\boldsymbol{\Delta}^{\text{sq}}$. Here we obtain four critical points, $F_1, \ldots, F_4$—one on each curve—which are depicted by small black circles in Fig. 2. By putting $\vartheta = \frac{\theta}{2}, \frac{\theta}{2} + \frac{\pi}{4}, \frac{\theta}{2} + \frac{2\pi}{4}$, and $\frac{\theta}{2} + \frac{3\pi}{4}$ in $(p_{(\vartheta)},q_{(\vartheta)})$ of (55), one has F_1, F_2, F_3, and F_4, in that order. Note that the F points are not the endpoints $E_1, \ldots, E_4$, which are shown only in Fig. 1, and not in Fig. 2.

The function $\boldsymbol{\Delta}^{\text{sq}}$ of (76) takes the value $2r$ at both points $\{F_2, F_4\}$ and takes the value $2(1-r)$ at $\{F_1, F_3\}$. So the global minimum is

$$\min\{2r\,,\, 2(1-r)\} \;\leqslant\; \boldsymbol{\Delta}^{\text{sq}}(\pm 1,p,\pm 1,q), \tag{77}$$

and thus we obtain a tight UR, like (54). One can confirm that the lower bound is

$$\begin{aligned} &2r \quad \text{if} \quad r \leqslant \tfrac{1}{2} \quad (\text{at } F_2, F_4 \text{ in Fig. 2}), \\ &2(1-r) \quad \text{if} \quad r \geqslant \tfrac{1}{2} \quad (\text{at } F_1, F_3 \text{ in Fig. 2}). \end{aligned} \tag{78}$$

Remark 3. The standard deviation $\Delta(\pm 1,p)$ is a concave function of p, hence the sum $\Delta(\pm 1,p) + \Delta(\pm 1,q)$ is a concave function on $\boldsymbol{\omega}$. As a result, we have another tight uncertainty relation:

$$\sqrt{1-(2r-1)^2} \;\leqslant\; \Delta(\pm 1,p) + \Delta(\pm 1,q). \tag{79}$$

One can check that the sum reaches its absolute minimum value at all the endpoints $E_1, \ldots, E_4$ and has its maximum value 2 at the center of $\boldsymbol{\omega}$. Both tight URs, (77) and (79), are known due to [26]. A quantum state that saturates a tight UR

is called its *minimum uncertainty state*. Since the E points and the F points are not the same, in general, the set—of minimum uncertainty states—is different for the two URs, (77) and (79), based on the standard deviation. Note that we always get the trivial lower bound $0 \leqslant \Delta(\mathbf{a},\vec{p})\Delta(\mathbf{b},\vec{q})$ for the product of standard deviations, and this bound can be reached by any ket that belongs to either of the bases given in (1).

Next, the Shannon entropy [41]

$$H(\vec{p}) = -\sum_{i=1}^{d} p_i \ln p_i \tag{80}$$

is arguably the most famous measure of uncertainty at present. It is superior to the standard deviation $\Delta(\mathbf{a},\vec{p})$ [10,11] because it depends only on $\vec{p}$, and not on the eigenvalues. One can show that $H(\vec{p}) \in [0, \ln d]$, and it is a concave function on Ω_a with the Hassian matrix composed of the second-order derivatives

$$\frac{\partial^2 H}{\partial p_k \partial p_l} = -\left(\frac{1}{p_l}\delta_{lk} + \frac{1}{p_d}\right) = \frac{\partial^2 H}{\partial p_l \partial p_k}, \tag{81}$$

where $p_d = 1 - \sum_{i=1}^{d-1} p_i$. Considering the same function for the b setting, that is, $H(\vec{q})$, one can formulate a combined uncertainty measure by the sum $H(\vec{p}) + H(\vec{q})$ and then produce an entropy UR [6–8]. Such URs are reviewed in [9–11]. For $d = 2$, the tight entropy UR is achieved in [27] and [29] (see also [28]), and we can directly import all those results here. In fact, Eq. (7) in [27] and Eq. (2.4) in [29] are $H(p) + H(q)$ on the ellipse, (55), and the absolute minimum of $H(p) + H(q)$ on the ellipse is found. In [29], all the results are given in terms of the angles between the real unit vectors, which are related to the angles between kets through (75).

We can choose

$$u_\gamma(\vec{p}) = \sum_{i=1}^{d} (p_i)^\gamma \quad \text{with} \quad 0 < \gamma < \infty \tag{82}$$

as another certainty or uncertainty measure, which is closely related to the Tsallis [35] and Rényi [39] entropies of order γ. One can prove that the Hassian matrix with entries

$$\frac{\partial^2 u_\gamma}{\partial p_k \partial p_l} = \gamma(\gamma-1)\left[{p_l}^{\gamma-2}\,\delta_{lk} + {p_d}^{\gamma-2}\right] = \frac{\partial^2 u_\gamma}{\partial p_l \partial p_k}, \tag{83}$$

$1 \leqslant k, l \leqslant d-1$, is a negative and positive semidefinite matrix for $0 < \gamma \leqslant 1$ and $1 \leqslant \gamma < \infty$, respectively. This confirms that $u_\gamma(\vec{p})$ is a concave (uncertainty) and convex (certainty) measure when $0 < \gamma \leqslant 1$ and $1 \leqslant \gamma < \infty$, respectively. A similar observation is made in [25] and [42]. In fact, our uncertainty measure $u(\vec{p})$ of (35) is $u_\gamma(\vec{p})$ with the exponent $\gamma = \frac{1}{2}$. Furthermore, the range of $u_\gamma(\vec{p})$ is $[1, d^{1-\gamma}]$ if $\gamma \leqslant 1$ and is $[d^{1-\gamma}, 1]$ if $1 \leqslant \gamma$. When $\gamma = 1$, $u_\gamma(\vec{p}) = 1$ for every $\vec{p} \in \Omega_a$ due to Eq. (5), thus u_1 is not a genuine certainty or uncertainty measure.

As before, one can establish a certainty or uncertainty relation with the sum $u_\gamma(\vec{p}) + u_\gamma(\vec{q})$. For $\gamma = 2$, in the case of $d = 2$, we obtain

$$u_2(p) + u_2(q) = 2 - \tfrac{1}{2}\mathbf{\Delta}^{\mathrm{sq}}(\pm 1, p, \pm 1, q)\,, \tag{84}$$

and then

$$u_2(p) + u_2(q) \leqslant \underbrace{2 - \min\{r\,,\,1-r\}}_{\max\{2-r,\,1+r\}} \tag{85}$$

as a tight certainty relation, which is also given in [17] for $\frac{1}{2} \leqslant r$. Due to (84), one can immediately derive (85) from the UR, (77). Where $\mathbf{\Delta}^{\mathrm{sq}}$ of (76) reaches its absolute minimum (uncertainty) on $\boldsymbol{\omega}$, there function (84) achieves its global maximum (certainty):

$$\max\{2-r, 1+r\} = \begin{cases} 2-r & \text{if} \quad r \leqslant \frac{1}{2} \quad (\text{at } F_2, F_4 \text{ in Fig. 2}), \\ 1+r & \text{if} \quad r \geqslant \frac{1}{2} \quad (\text{at } F_1, F_3 \text{ in Fig. 2}). \end{cases} \tag{86}$$

The certainty measure, (84), hits its absolute minimum 1 at the center of $\boldsymbol{\omega}$ (depicted by the black star in Figs. 1 and 2).

Remark 4. One can have another tight certainty relation,

$$u_2(p)\,u_2(q) \leqslant \tfrac{1}{4}\max\{(2-r)^2, (1+r)^2\}, \tag{87}$$

where the product of certainty measures is used. Relation (87) is presented in [17] for $\frac{1}{2} \leqslant r$. One can verify that $u_2(p)u_2(q)$ is a convex function on $\boldsymbol{\omega}$. Therefore, its absolute maximum [given in (87)] will be on the ellipse [specified by (55)], and the global minimum $\frac{1}{4}$ will be at the center of $\boldsymbol{\omega}$. The product function reaches its upper bound at the F points. By applying the negative of the logarithm on both sides of inequality (87), we get the corresponding tight UR—achieved in [30]—in terms of the collision entropy (that is, the Rényi entropy [39] of order 2).

Finally, we pick the function

$$u_{\max}(\vec{p}) = \max_{1 \leqslant i \leqslant d} \{p_i\}, \tag{88}$$

which defines the norm on $\mathbb{R}^d$ if we replace p_i with $|p_i|$. Since every p_i follows (6), the modulus sign is not shown in (88). Every norm is a convex function, so $u_{\max}$ can be considered a certainty measure on Ω_a; $u_{\max}(\vec{p}) \in [\frac{1}{d}, 1]$ for every $\vec{p} \in \Omega_a$. Note that $u_{\max}(\vec{p})$ is not differentiable everywhere in Ω_a. Nevertheless, we can assemble a combined certainty measure with the sum $u_{\max}(\vec{p}) + u_{\max}(\vec{q})$ on $\boldsymbol{\omega}$.

In the case of $d = 2$, the function $u_{\max}(p) + u_{\max}(q)$ is equal to

$$\begin{array}{llllll} (1-p)+(1-q) & \text{if} & 0 \leqslant p \leqslant \frac{1}{2} & \text{and} & 0 \leqslant q \leqslant \frac{1}{2}, \\ (1-p)+q & \text{if} & 0 \leqslant p \leqslant \frac{1}{2} & \text{and} & \frac{1}{2} \leqslant q \leqslant 1, \\ p+(1-q) & \text{if} & \frac{1}{2} \leqslant p \leqslant 1 & \text{and} & 0 \leqslant q \leqslant \frac{1}{2}, \\ p+q & \text{if} & \frac{1}{2} \leqslant p \leqslant 1 & \text{and} & \frac{1}{2} \leqslant q \leqslant 1. \end{array} \tag{89}$$

The limits on p and q stated in (89) divide $\boldsymbol{\omega}$—which is an elliptical region (see Figs. 1 and 2)—into four quadrants. The

function $u_{\max}(p)+u_{\max}(q)$ is differentiable in each of the quadrants. Furthermore, since it is a convex function on $\boldsymbol{\omega}$, its global maximum will be at the ellipse, (55). Here we discover four critical points, one in each quadrant on the ellipse, where the combined function takes a maximum value. In fact, these four points are the same $F_1,\ldots,F_4$ shown in Fig. 2.

The combined measure acquires the value $1+\sqrt{1-r}$ at both F_2 and F_4 and reaches the value $1+\sqrt{r}$ at both F_1 and F_3. Thus, like (85), we get the tight certainty relation

$$u_{\max}(p)+u_{\max}(q)\leqslant \max\{1+\sqrt{1-r}\,,1+\sqrt{r}\,\} \tag{90}$$

for a qubit. And the absolute maximum (upper bound) is given by

$$\begin{array}{lll} 1+\sqrt{1-r} & \text{if} \quad r\leqslant \frac{1}{2} & (\text{at } F_2,F_4 \text{ in Fig. 2}),\\ 1+\sqrt{r} & \text{if} \quad r\geqslant \frac{1}{2} & (\text{at } F_1,F_3 \text{ in Fig. 2}), \end{array} \tag{91}$$

analogous to (86). Besides, $u_{\max}(p)+u_{\max}(q)$ has its global minimum 1 at the center of $\boldsymbol{\omega}$ (shown by the black star in Figs. 1 and 2).

The certainty relation, (90), is captured in [31] using the inequality

$$\arccos\left(\max_{ij}\sqrt{r_{ij}}\right)\leqslant \arccos\left(\max_{i}\sqrt{p_i}\right)+\arccos\left(\max_{j}\sqrt{q_j}\right). \tag{92}$$

Instead of TIs, (53), for a qubit, all the tight relations, (54), (69), (77), (79), (85), (87), (90), (93), and (94), and the entropy UR given in [27–29] can be obtained with (92). In fact, inequality (92), that is, $\min_{ij}\theta_{ij}\leqslant \min_i\alpha_i+\min_j\beta_j$, can be produced from d^2 TIs, (13), and it is weaker than the TIs: all the $(\vec{p},\vec{q})\in\Omega$ that are bounded by (92) rather than (13) constitute a bigger combined-probability space.

Remark 5. One can confirm that the product $u_{\max}(p)u_{\max}(q)$ is neither a concave nor a convex function on $\boldsymbol{\omega}$ (for a similar observation, see [8]), so it not clear to us whether or not we can take it as a good combined-certainty or combined-uncertainty measure for every qubit's state. It also shows that the product of two convex (concave) functions is not necessarily a convex (concave) function. By computing the gradient of $u_{\max}(p)u_{\max}(q)$ in each of the four quadrants, one realizes that the function reaches its global minimum $\frac{1}{4}$ at the center of $\boldsymbol{\omega}$ and reaches its global maximum (on the ellipse) at the F points. Hence, we have the tight relation

$$u_{\max}(p)\,u_{\max}(q)\leqslant \tfrac{1}{4}\max\{(1+\sqrt{1-r})^2,(1+\sqrt{r})^2\}, \tag{93}$$

which is reported in [8] (and implicitly appears in [6]). In fact, for $d=2$, the ket given by Eq. (11) in [6] is ket (A14) with $\beta=\frac{\theta}{2}$ and $\nu=0$, and the ket corresponds to point F_1. By applying the negative of the logarithm on both sides of inequality (93), one can transform this relation into min-entropy terms [24]. The min-entropy $H_{\min}(q):=-\ln\left(u_{\max}(q)\right)$ is the lowest in the family of Rényi entropies [39], and it is neither a concave nor a convex function on the interval $[0,1]$. As above, using the min-entropy, one can have another tight relation,

$$-\ln\left(\max\{r,1-r\}\right)\leqslant H_{1/2}(p)+H_{\min}(q), \tag{94}$$

which is also given in [8]; recall that $H_{1/2}(p)=2\ln\left(u(p)\right)$. The function $H_{1/2}(p)+H_{\min}(q)$ always takes its global minimum at the endpoints E_2 and E_4 and takes its absolute maximum $2\ln 2$ at the center (shown in Fig. 1) of $\boldsymbol{\omega}$. In [32], a general expression for the tight lower bound of a sum of Rényi entropies is given, which is basically the minimization of the sum on the ellipse.

V. CONCLUSION AND OUTLOOK

Taking the pure quantum state for a qudit, we present TIs, (13), and then the combined-probability space $\boldsymbol{\omega}$ for a general pair of measurement settings. The combined space is a compact and convex set in $\mathbb{R}^{2d}$, and all its extreme points are represented by m-parametric curves, $1\leqslant m\leqslant d-1$. These curves are determined by two settings (Θ matrix) and are sufficient to generate the whole $\boldsymbol{\omega}$ as well as to provide a certainty or uncertainty relation.

One can pick some suitable concave and convex functions on $\boldsymbol{\omega}$ to quantify the uncertainty and certainty, respectively. Subsequently, one can establish an uncertainty (a certainty) relation by finding the absolute minimum (maximum) of a function at the parametric curves. Due to the parametric curves, the formulation of a certainty or uncertainty relation becomes a single-parameter optimization problem.

Particularly for the uncertainty measures, (38) and (64), the absolute minima can always be easily computed by repeating the three-step procedure given in Sec. III with every M set, $2\leqslant \text{M}\leqslant d$, built with entries in the Θ matrix. And, thus, one can obtain the corresponding URs for any pair of measurement settings. For the other functions, one needs to find first all the critical points on the curves and then the absolute extrema at those points. That is still much easier than searching for the extrema in the whole space. In each case, the extremum—which is the lower (upper) bound on an uncertainty (certainty) measure—depends only on the measurement settings, and not on a quantum state. Every (pure or mixed) state of a qudit provides a point in $\boldsymbol{\omega}$ by the Born rule and respects every certainty and uncertainty relation presented here.

In the case of a qubit, $d=2$, we show that many known tight certainty and uncertainty relations, owing to [6,8,17] and [25–32], can be derived from the TIs, (53). These TIs define an ellipse that represents all the parametric curves, and each point on the ellipse (and in $\boldsymbol{\omega}$) corresponds to a qubit's state, thus we have tight relations. The same ellipse also emerges in [16–18] as a special case. For a pair of measurement settings on a qubit, it seems that the TIs, (13), and the results in [13] and [16–18] provide more fundamental QCs than the tight certainty and uncertainty relations.

The TIs, (13), do not provide all possible QCs when the dimension $d>2$, hence there are still some points in $\boldsymbol{\omega}$ that correspond to no quantum state, and our URs given in Sec. III are not tight in general. However, all our certainty and uncertainty relations are built on the fact that "every point outside of $\boldsymbol{\omega}$ is, surely, not associated with any quantum state." One can include other QCs, namely, TIs, (12); then the domain $\boldsymbol{\omega}$ of the certainty or uncertainty function will be smaller. Consequently, better bounds and finer certainty and uncertainty relations can be achieved. To get a tight bound, in the case of general settings and $d>2$, is a challenging task. Tight URs are only known in some special cases: the position momentum [3], MUBs [7,8,17,21,22,24], and the qubit [6,8,17,25–32].

URs have numerous applications in different strands of physics. Recently, these have been employed for certain quantum information processing tasks such as cryptography [24] and entanglement detection [31,43–46]. As our certainty and uncertainty relations arise solely from TIs, one can directly appoint TIs, (12), as genuine QCs for this job. Furthermore, in quantum state estimation [47], one collects data by applying different measurement settings, thus realizing scheme (2) in a laboratory. Then $\rho_{\rm est}$ is constructed with the data. There one needs to confirm that the estimated $\rho_{\rm est}$ represents a legitimate quantum state. Again, TIs, (12), could be utilized for such a test, for instance, one can first check whether or not the estimated $(\vec{p}_{\rm est},\vec{q}_{\rm est})$ follows all the TIs.

ACKNOWLEDGMENTS

I am very grateful to Arvind for stimulating discussions and helpful comments on the manuscript. I thank Arun Kumar Pati for bringing Refs. [13] and [31] to my attention and Jędrzej Kaniewski for explaining and making me aware of their work [18].

APPENDIX A: DERIVATION OF THE TRIANGLE INEQUALITIES

Landau and Pollak obtained a single TI of the kind given in (13) for continuous-time signals. One can spot several similarities between their work [13] and the following derivation. In this paper, the primary QCs are the TIs, (12). To derive these TIs, we consider three kets, $|\psi\rangle$, $|a\rangle$, and $|b\rangle$, of a d-dimensional Hilbert space $\mathscr{H}_d$. Their inner products are expressed in the polar form as

$$\langle a|\psi\rangle := \sqrt{p}\, e^{\mathrm{i}\mu} = \cos\alpha\, e^{\mathrm{i}\mu}, \tag{A1}$$

$$\langle b|\psi\rangle := \sqrt{q}\, e^{\mathrm{i}\nu} = \cos\beta\, e^{\mathrm{i}\nu}, \quad \text{and} \tag{A2}$$

$$\langle a|b\rangle := \sqrt{r}\, e^{\mathrm{i}\delta} = \cos\theta\, e^{\mathrm{i}\delta}, \tag{A3}$$

where the phases $\mu,\nu,\delta \in [0,2\pi)$. In the text, $|\psi\rangle$ is associated with a quantum state, and $|a\rangle$ and $|b\rangle$ with the two measurement settings [see (1)]. Through the inner products, the quantum angles α, β, and θ are related to the probabilities p, q, and r [see also (3), (4), (9), and (10)], and $\mathrm{i} = \sqrt{-1}$. Recall that the angles lie in $[0,\frac{\pi}{2}]$, and the probabilities belong to the interval $[0,1]$.

It is always feasible to write one ket, say $|\psi\rangle$, as a sum of its component in the linear span of the other two, $\{|a\rangle,|b\rangle\}$, and its component in the orthogonal complement of the span [see (A6)]. In general, $|a\rangle$ and $|b\rangle$ are not orthogonal to each other. In the case of $0 < |\langle a|b\rangle| < 1$, employing the Gram-Schmidt orthogonalization process, one can convert the linearly independent set $\{|a\rangle,|b\rangle\}$ into an orthonormal set $\{|b\rangle,|b^{\perp}\rangle\}$ or $\{|a\rangle,|a^{\perp}\rangle\}$, where

$$|b^{\perp}\rangle = \frac{|a\rangle - \langle b|a\rangle|b\rangle}{\sqrt{1-|\langle a|b\rangle|^2}} \quad \text{and} \quad |a^{\perp}\rangle = \frac{|b\rangle - \langle a|b\rangle|a\rangle}{\sqrt{1-|\langle a|b\rangle|^2}}. \tag{A4}$$

The two sets are related by a unitary transformation:

$$\begin{pmatrix} |b\rangle \\ |b^{\perp}\rangle \end{pmatrix} = \begin{pmatrix} \langle a|b\rangle & \sqrt{1-|\langle a|b\rangle|^2} \\ \sqrt{1-|\langle a|b\rangle|^2} & -\langle b|a\rangle \end{pmatrix} \begin{pmatrix} |a\rangle \\ |a^{\perp}\rangle \end{pmatrix}. \tag{A5}$$

Now we can resolve

$$|\psi\rangle = \cos\beta\, e^{\mathrm{i}\nu}|b\rangle + \langle b^{\perp}|\psi\rangle|b^{\perp}\rangle + \langle x|\psi\rangle|x\rangle \tag{A6}$$

with a suitable ket $|x\rangle$ that follows $\langle b|x\rangle = 0 = \langle b^{\perp}|x\rangle$. If and only if $|\psi\rangle$ lies in the span of $\{|a\rangle,|b\rangle\}$, the last term in the expansion, (A6), vanishes; otherwise, not. With the normalization of $|\psi\rangle$, one can recognize $|\langle b^{\perp}|\psi\rangle|^2 + |\langle x|\psi\rangle|^2 = (\sin\beta)^2$, and subsequently

$$0 \leqslant |\langle x|\psi\rangle| \Rightarrow |\langle b^{\perp}|\psi\rangle| \leqslant \sin\beta. \tag{A7}$$

Taking the transformation, (A5), and the polar form, (A3), we realize another representation of the ket

$$\begin{aligned} |\psi\rangle = {} & (\cos\theta\cos\beta\, e^{\mathrm{i}(\nu+\delta)} + \sin\theta\,\langle b^{\perp}|\psi\rangle)\,|a\rangle \\ & + (\sin\theta\cos\beta\, e^{\mathrm{i}\nu} - \cos\theta e^{-\mathrm{i}\delta}\langle b^{\perp}|\psi\rangle)|a^{\perp}\rangle \\ & + \langle x|\psi\rangle|x\rangle \end{aligned} \tag{A8}$$

from (A6). With the new representation, (A8), and the polar form

$$\langle b^{\perp}|\psi\rangle := |\langle b^{\perp}|\psi\rangle|\, e^{\mathrm{i}\xi}, \quad \xi \in [0,2\pi), \tag{A9}$$

we attain

$$\begin{aligned} p = |\langle a|\psi\rangle|^2 = {} & (\cos\theta\,\cos\beta)^2 + (\sin\theta)^2\,|\langle b^{\perp}|\psi\rangle|^2 \\ & + 2\cos\theta\sin\theta\cos\beta\,|\langle b^{\perp}|\psi\rangle| \\ & \times \cos(\xi - (\nu+\delta)). \end{aligned} \tag{A10}$$

Remember that $\langle a|x\rangle = 0 = \langle a^{\perp}|x\rangle$ because $|x\rangle$ lies in the orthogonal complement of $\{|a\rangle,|b\rangle\}$. Owing to

$$\cos(\xi - (\nu+\delta)) \leqslant 1, \tag{A11}$$

first, we obtain the left-hand-side inequality in

$$p \leqslant (\cos\theta\cos\beta + \sin\theta|\langle b^{\perp}|\psi\rangle|)^2 \leqslant [\cos(\theta-\beta)]^2 \tag{A12}$$

and, afterwards, the right-hand-side inequality with the aid of (A7). Eventually, from above, we have

$$p = (\cos\alpha)^2 \leqslant [\cos(\theta-\beta)]^2 \tag{A13}$$

[using the polar form (A1)].

If there are equalities in (A11) as well as in (A7), then we reach an equality—in the place of an inequality—in (A13): $\xi = \nu+\delta \pmod{2\pi}$ are the solutions of the equation $\cos(\xi-(\nu+\delta)) = 1$. And $|\langle x|\psi\rangle| = 0$ implies that $|\psi\rangle$ is contained in the subspace generated by $\{|a\rangle,|b\rangle\}$, thus $|\langle b^{\perp}|\psi\rangle| = \sin\beta$. Under these two conditions, (A6) and (A8) become

$$|\psi\rangle = e^{\mathrm{i}\nu}[\cos\beta\,|b\rangle + \sin\beta\, e^{\mathrm{i}\delta}\,|b^{\perp}\rangle] \tag{A14}$$

$$= e^{\mathrm{i}\nu}[\cos(\theta-\beta)\, e^{\mathrm{i}\delta}|a\rangle + \sin(\theta-\beta)\,|a^{\perp}\rangle]. \tag{A15}$$

These $|\psi\rangle$ kets—where δ is specified by the polar form, (A3), provided $\langle a|b\rangle \neq 0$, and the global phase ν can be any real number—are the only kets that saturate inequality (A13). We cannot straightforwardly use the above analysis for the next two cases, $|\langle a|b\rangle| = 0,1$, hence these are studied individually.

In the case of $\langle a|b\rangle = 0$, $|b^{\perp}\rangle = |a\rangle$ and $|a^{\perp}\rangle = |b\rangle$; in fact, there is no need for the orthogonalization process, and both representations, (A6) and (A8), of $|\psi\rangle$ become the same. Furthermore, δ is not determined by the polar form, (A3), whereas $\theta = \frac{\pi}{2}$. Now the inequality, (A13), becomes $(\cos\alpha)^2 + (\cos\beta)^2 \leqslant 1$, which is—directly realized from (A6) due to (A7)—saturated by ket (A14) with an arbitrary real phase δ [remember that $\cos\alpha = |\langle a|\psi\rangle|$ due to (A1)].

In the case of $|\langle a|b\rangle| = 1$, $\theta = 0$ and $|b\rangle = e^{i\delta}|a\rangle$ according to (A3), and the above orthogonalization process, and thus $|b^{\perp}\rangle$ and $|a^{\perp}\rangle$, does not exist. Consequently, the term $\langle b^{\perp}|\psi\rangle|b^{\perp}\rangle$ will not then appear in the decomposition, (A6), of $|\psi\rangle$. In the places of (A7), (A13), and (A14) we have $0 \leqslant |\langle x|\psi\rangle| \Rightarrow (\cos\beta)^2 \leqslant 1$, $(\cos\alpha)^2 = (\cos\beta)^2$, and $|\psi\rangle = e^{i\nu}|b\rangle$, respectively. In this case, there is no genuine QC, nevertheless, $(\cos\beta)^2 \leqslant 1$ is saturated by the ket(s) $|\psi\rangle = e^{i\nu}|b\rangle$ [remember that $\cos\beta = |\langle b|\psi\rangle|$; see (A2)].

One can appreciate that inequality (A13) is a legitimate QC, and α and β must respect that for every $\theta \in [0, \frac{\pi}{2}]$. Applying the square root to both sides of the inequality, we obtain

$$\cos\alpha = |\cos\alpha| \leqslant |\cos(\theta - \beta)| = \cos(\theta - \beta). \tag{A16}$$

Since $\alpha \in [0, \frac{\pi}{2}]$ and $(\theta - \beta) \in [-\frac{\pi}{2}, \frac{\pi}{2}]$, both $\cos\alpha$ and $\cos(\theta - \beta)$ are nonnegative numbers, hence there is no need to use the modulus on either side of the above inequality. As the arccos function is a strictly decreasing function and $\arccos(\cos\varsigma) = |\varsigma|$ for $\varsigma \in [-\frac{\pi}{2}, \frac{\pi}{2}]$, from (A16) we get an equivalent form,

$$|\theta - \beta| \leqslant \alpha, \tag{A17}$$

of (A13). In fact, (A17) carries two TIs: $\theta \leqslant \alpha + \beta$ and $\beta \leqslant \alpha + \theta$. $|\psi\rangle$ of (A14) with $0 \leqslant \beta \leqslant \theta$ saturates the TI $\theta \leqslant \alpha + \beta$, and with $\theta \leqslant \beta \leqslant \frac{\pi}{2}$ it saturates the other TI, $\beta \leqslant \alpha + \theta$. TIs such as $\theta \leqslant \alpha + \beta$ [see (13)] are used to define the combined-probability space $\boldsymbol{\omega}$ in Sec. II.

Replacing the ordered set $\{b,\beta,\nu\}$ by $\{a,\alpha,\mu\}$ in (A6) and repeating the above analysis, one will discover

$$q = (\cos\beta)^2 \leqslant [\cos(\theta - \alpha)]^2 \quad \text{and} \tag{A18}$$

$$|\theta - \alpha| \leqslant \beta \tag{A19}$$

in the places of (A13) and (A17), respectively. Jointly, (A17) and (A19) can be written as

$$|\theta - \beta| \leqslant \alpha \leqslant \theta + \beta, \tag{A20}$$

which displays three TIs associated with the three angles. A TI states: *The sum of two quantum angles must be greater than or equal to the remaining quantum angle.*

In fact, the quantum angle "$\arccos|\langle\,|\,\rangle|$" is a metric (and a distinguishability measure [12]) on the set $\mathcal{S}_{\text{pure}}$ of all pure states ($\rho = \rho^2$). This is because the four conditions,

(i) $\arccos|\langle a|b\rangle| \geqslant 0$,

(ii) $\arccos|\langle a|b\rangle| = 0$ if and only if $|a\rangle\langle a| = |b\rangle\langle b|$,

(iii) $\arccos|\langle a|b\rangle| = \arccos|\langle b|a\rangle|$, and

(iv) $\arccos|\langle a|b\rangle| \leqslant \arccos|\langle a|\psi\rangle| + \arccos|\langle\psi|b\rangle|$,

are satisfied for every $|a\rangle\langle a|$, $|b\rangle\langle b|$, and $|\psi\rangle\langle\psi|$ in $\mathcal{S}_{\text{pure}}$, where $|\langle a|b\rangle| = \sqrt{\text{tr}(|a\rangle\langle a|\,|b\rangle\langle b|)}$. Note that every pure state ρ on $\mathscr{H}_d$ is made of a ket in $\mathscr{H}_d$, and two kets that are equal up to a global phase provide the same pure state. As the arccos function is nonnegative, the first condition is valid. The second and third are true by virtue of $|\langle a|b\rangle| = 1 \Leftrightarrow |a\rangle\langle a| = |b\rangle\langle b|$ and $|\langle a|b\rangle| = |\langle b|a\rangle|$, respectively. The last condition is the TI $\theta \leqslant \alpha + \beta$, derived above.

Returning to the TIs, (A20), as $\alpha \in [0, \frac{\pi}{2}]$, $\theta + \beta$ will be a true upper bound on α only if it is smaller than or equal to $\frac{\pi}{2}$. Hence, we can further improve (A20) as

$$|\theta - \beta| \leqslant \alpha \leqslant \min\left\{\theta + \beta, \frac{\pi}{2}\right\}. \tag{A21}$$

Taking the right-hand-side inequality and applying the cosine function—which decreases monotonically on $[0,\pi]$—to both the terms, we get

$$\max\{\cos(\theta + \beta), 0\} \leqslant \cos\alpha. \tag{A22}$$

Now, considering Heaviside's unit step function

$$\eta(\upsilon) := \begin{cases} 0 & \text{if} \quad \upsilon < 0, \\ 1 & \text{if} \quad \upsilon \geqslant 0, \end{cases} \tag{A23}$$

one can rewrite (A22) as

$$\eta(\cos(\theta + \beta))\cos(\theta + \beta) \leqslant \cos\alpha. \tag{A24}$$

Since the terms on either side of the above inequality are nonnegative, squaring both sides delivers

$$\eta(\cos(\theta + \beta))[\cos(\theta + \beta)]^2 \leqslant (\cos\alpha)^2. \tag{A25}$$

Putting (A13) and (A25) side by side, we obtain

$$\eta(\cos(\theta + \beta))[\cos(\theta + \beta)]^2 \leqslant (\cos\alpha)^2 \leqslant [\cos(\theta - \beta)]^2. \tag{A26}$$

Furthermore, due to (A1)–(A3), (A26) becomes

$$\eta(\tau_-)\,{\tau_-}^2 \leqslant p \leqslant {\tau_+}^2, \tag{A27}$$

where

$$\tau_- := \sqrt{r\,q} - \sqrt{(1-r)(1-q)} \quad \text{and} \tag{A28}$$

$$\tau_+ := \sqrt{r\,q} + \sqrt{(1-r)(1-q)}. \tag{A29}$$

In essence, we obtain QCs (A21) and (A27), which are equivalent to each other; one is in terms of the quantum angles and the other is in terms of the probabilities.

APPENDIX B: COMPACTNESS AND CONVEXITY OF $\boldsymbol{\omega} \subset \boldsymbol{\Omega}$

The real vector space $\mathbb{R}^{2d}$ is also a metric space with the Euclidean distance, and both its subsets, Ω and $\boldsymbol{\omega}$, are closed as well as bounded, hence they are compact sets (thanks to the Heine-Borel theorem; see in [48]). Since a convex combination of probability vectors is again a probability vector, both Ω_a and Ω_b are convex subsets of $\mathbb{R}^d$. Moreover, $\Omega = \Omega_a \times \Omega_b$ is a convex set because it is a Cartesian product of two such sets.

To prove the convexity of $\boldsymbol{\omega}$, we consider two combined vectors, $(\vec{p}\,',\vec{q}\,')$ and $(\vec{p}\,'',\vec{q}\,'')$, that belong to $\boldsymbol{\omega}$. This means that their components follow constraints (5)–(8) and (15); that is,

$$p_i' + q_j' \leqslant r_{ij} + 1 + 2\sqrt{r_{ij}(1-p_i')(1-q_j')}, \tag{B1}$$

$$p_i'' + q_j'' \leqslant r_{ij} + 1 + 2\sqrt{r_{ij}(1-p_i'')(1-q_j'')} \tag{B2}$$

for every $1 \leqslant i,\ j \leqslant d$. For the proof, we need to show that a convex combination

$$(\vec{p},\vec{q}) = \lambda\,(\vec{p}\,',\vec{q}\,') + (1-\lambda)(\vec{p}\,'',\vec{q}\,'') \tag{B3}$$

fulfills all the requirements, (5)–(8) and (15), and therefore lies in $\boldsymbol{\omega}$, for every $\lambda \in [0,1]$. Thanks to the convexity of Ω, the combination, (B3), belongs to Ω and $(\vec{p},\vec{q})$ meets all the demands, (5)–(8).

Now we demonstrate that the components p_i and q_j of $(\vec{p},\vec{q})$ respect inequality (15):

$$\begin{aligned} p_i + q_j &= \lambda\,(p_i' + q_j') + (1-\lambda)(p_i'' + q_j'') && \text{(B4)}\\ &\leqslant r_{ij} + 1 + 2\sqrt{r_{ij}}\,\Big[\lambda\sqrt{(1-p_i')(1-q_j')} \\ &\quad + (1-\lambda)\sqrt{(1-p_i'')(1-q_j'')}\Big] && \text{(B5)}\\ &\leqslant r_{ij} + 1 + 2\sqrt{r_{ij}}\,\sqrt{1-\lambda p_i' - (1-\lambda)p_i''} \\ &\quad \times \sqrt{1-\lambda q_j' - (1-\lambda)q_j''} && \text{(B6)}\\ &= r_{ij} + 1 + 2\sqrt{r_{ij}}\sqrt{(1-p_i)(1-q_j)}. && \text{(B7)} \end{aligned}$$

We have equality (B4) due to the convex combination (B3), and then we obtain inequality (B5) by employing (B1) and (B2). The next inequality, (B6), is attributed to the concavity of a real-valued function,

$$f(p,q) := \sqrt{(1-p)(1-q)}, \tag{B8}$$

defined on $[0,1]\times[0,1]$, and the last equality is again because of combination (B3). In conclusion, the combined-probability space $\boldsymbol{\omega}$ is a convex set in $\mathbb{R}^{2d}$. In addition, to recognize that $f(p,q)$ is a concave function, we present the Hessian matrix

$$\begin{pmatrix} \frac{\partial^2 f}{\partial p^2} & \frac{\partial^2 f}{\partial p\partial q} \\ \frac{\partial^2 f}{\partial q\partial p} & \frac{\partial^2 f}{\partial q^2} \end{pmatrix} = \begin{pmatrix} \frac{-(1-q)^{1/2}}{4(1-p)^{3/2}} & \frac{1}{4(1-p)^{1/2}(1-q)^{1/2}} \\ \frac{1}{4(1-p)^{1/2}(1-q)^{1/2}} & \frac{-(1-p)^{1/2}}{4(1-q)^{3/2}} \end{pmatrix}, \tag{B9}$$

which is a negative semidefinite matrix for every p and q in the interval $[0,1)$. For $p=1$, or $q=1$, or both, $f(p,q)=0$, and the Hessian matrix is the 2×2 zero matrix.

APPENDIX C: PRELIMINARY CALCULATIONS FOR APPENDIX D

With (3), (4), (9), and (10), let us again acknowledge that probability $=[\cos(\text{angle})]^2$, and the quantum angles belong to the interval $[0,\frac{\pi}{2}]$. Now we consider $j \neq l$ and

$$\begin{aligned} q_j + q_l &= (\cos\beta_j)^2 + (\cos\beta_l)^2 \\ &= 1 + \cos(\beta_j+\beta_l)\cos(\beta_j-\beta_l). && \text{(C1)} \end{aligned}$$

Since the difference between angles $\beta_j - \beta_l \in [-\frac{\pi}{2},\frac{\pi}{2}]$, we have $0 \leqslant \cos(\beta_j-\beta_l)$. Hence, with (C1), one can establish that

$$q_j + q_l \leqslant 1 \ \Leftrightarrow\ \cos(\beta_j+\beta_l) \leqslant 0, \tag{C2}$$

and then

$$q_j + q_l \leqslant 1 \ \Leftrightarrow\ \frac{\pi}{2} \leqslant \beta_j + \beta_l \quad (j \neq l) \tag{C3}$$

due to the arccos function; note that $\arccos(\cos\varsigma) = \varsigma$ for $\varsigma \in [0,\pi]$. One can also perceive $\frac{\pi}{2} \leqslant \beta_j + \beta_l$ as a TI.

Next we validate a result that is applied in Appendix D:

$$\begin{aligned} &\text{If } j \neq l,\ 0 \leqslant \theta_{ij} - \beta_j, \quad \text{and} \quad 0 \leqslant \theta_{kl} - \beta_l, \ \text{then} \\ &1 \leqslant [\cos(\theta_{ij}-\beta_j)]^2 + [\cos(\theta_{kl}-\beta_l)]^2. && \text{(C4)} \end{aligned}$$

Let us designate $\theta_{ij}-\beta_j$ and $\theta_{kl}-\beta_l$ by φ_{ij} and φ_{kl}, respectively, and write

$$(\cos\varphi_{ij})^2 + (\cos\varphi_{kl})^2 = 1 + \cos(\varphi_{ij}+\varphi_{kl})\cos(\varphi_{ij}-\varphi_{kl}) \tag{C5}$$

just like (C1). One can show that the sum

$$\varphi_{ij} + \varphi_{kl} = (\theta_{ij}+\theta_{kl}) - (\beta_j+\beta_l) \leqslant \frac{\pi}{2} \tag{C6}$$

due to $\theta_{ij}+\theta_{kl} \leqslant \pi$ and (C3). Clearly, $\varphi_{ij},\varphi_{kl} \leqslant \frac{\pi}{2}$ because $\theta,\beta \in [0,\frac{\pi}{2}]$, and if $0 \leqslant \varphi_{ij},\varphi_{kl}$ [see the requirements in (C4)], then we have $0 \leqslant \varphi_{ij}+\varphi_{kl}$ and $\varphi_{ij}-\varphi_{kl} \in [-\frac{\pi}{2},\frac{\pi}{2}]$. As the net result, $0 \leqslant \cos(\varphi_{ij} \pm \varphi_{kl})$, the last term in (C5) turns out to be a nonnegative function, and thus we obtain $1 \leqslant (\cos\varphi_{ij})^2 + (\cos\varphi_{kl})^2$. This completes the proof of (C4).

In addition to the requirements in (C4), if and only if

$$\theta_{ij} = \frac{\pi}{2} = \theta_{kl} \quad \text{and} \quad \beta_j + \beta_l = \frac{\pi}{2},$$

then we acquire the equality

$$1 = [\cos(\theta_{ij}-\beta_j)]^2 + [\cos(\theta_{kl}-\beta_l)]^2 \ \text{in (C4)}. \tag{C7}$$

If $\theta_{ij} = \frac{\pi}{2} = \theta_{kl}$ and $\beta_j + \beta_l = \frac{\pi}{2}$, then evidently we have the equality of (C7). Now let us prove the converse under the requirements $0 \leqslant \varphi_{ij},\varphi_{kl}$ of (C4). If $(\cos\varphi_{ij})^2 + (\cos\varphi_{kl})^2 = 1$, then the last term in (C5) must vanish, which occurs—provided $0 \leqslant \varphi_{ij},\varphi_{kl}$—when the sum in (C6) attains its upper bound $\frac{\pi}{2}$ or $\varphi_{ij}-\varphi_{kl} = \pm\frac{\pi}{2}$. The case $\varphi_{ij}-\varphi_{kl} = \frac{\pi}{2}$ arises when $\varphi_{ij} = \frac{\pi}{2}$ and $\varphi_{kl} = 0$, and $\varphi_{ij}-\varphi_{kl} = -\frac{\pi}{2}$ occurs when $\varphi_{ij} = 0$ and $\varphi_{kl} = \frac{\pi}{2}$. Both these cases occur under $\varphi_{ij}+\varphi_{kl} = \frac{\pi}{2}$—that is, when the sum in (C6) reaches its upper bound—which materializes if and only if $\theta_{ij} = \frac{\pi}{2} = \theta_{kl}$ and $\beta_j + \beta_l = \frac{\pi}{2}$; this validates (C7).

Similarly to (C3) we have

$$p_i + p_k \leqslant 1 \ \Leftrightarrow\ \frac{\pi}{2} \leqslant \alpha_i + \alpha_k \quad (i \neq k), \tag{C8}$$

and similarly to (C4) plus (C7) we have the following:

$$\begin{aligned} &\text{If} \quad i \neq k, \quad 0 \leqslant \theta_{ij} - \alpha_i, \quad \text{and} \quad 0 \leqslant \theta_{kl} - \alpha_k, \\ &\text{then} \quad 1 \leqslant [\cos(\theta_{ij}-\alpha_i)]^2 + [\cos(\theta_{kl}-\alpha_k)]^2. \end{aligned}$$

In addition, if and only if

$$\theta_{ij} = \frac{\pi}{2} = \theta_{kl} \quad \text{and} \quad \alpha_i + \alpha_k = \frac{\pi}{2},$$

then we own the equality

$$1 = [\cos(\theta_{ij}-\alpha_i)]^2 + [\cos(\theta_{kl}-\alpha_k)]^2. \tag{C9}$$

APPENDIX D: EXTREME POINTS OF $\boldsymbol{\omega}$

In Appendix B, we demonstrate that the combined-probability space $\boldsymbol{\omega}$ is a compact convex set in $\mathbb{R}^{2d}$. According to the Krein-Milman theorem (see Theorem 3.3.5

and Appendix A.3 in [15]), every point in such a set can be decomposed into a convex combination of its extreme points. In this Appendix, starting from an arbitrary interior point of $\boldsymbol{\omega}$, we move toward its extreme points.

1. Interior of $\boldsymbol{\omega}$

A point $(\vec{p},\vec{q}) \in \boldsymbol{\omega}$ that obeys each of the constraints (6), (8), and (13) with *strict* inequality,

$$0 < \dot{p}_i, \quad 0 < \dot{q}_j, \quad \theta_{ij} < \dot{\alpha}_i + \dot{\beta}_j \quad \text{for all} \quad 1 \leqslant i, j \leqslant d, \tag{D1}$$

is called an *interior* point of $\boldsymbol{\omega}$. In certain cases, such as $d = 2$ and $\theta \in \{0, \frac{\pi}{2}\}$, there exist only extreme points, and no interior point; then the following analysis is not needed. However, for $d > 2$, there is always an interior point: with $\theta_{ij} \leqslant \frac{\pi}{2} < 2 \arccos \frac{1}{\sqrt{d}}$, one can show that the center—specified by $p_i = \frac{1}{d} = q_j$ for all i, j—of $\boldsymbol{\omega}$ is an interior point when $d > 2$.

We begin our journey from a general but fixed interior point $(\vec{p},\vec{q})$ along a straight line, which is the locus of points $\vec{P} = (p_1, p_2, \vec{p}_{\text{rest}}, \vec{q}) \in \mathbb{R}^{2d}$, where p_1, p_2 obey the linear equation

$$p_1 + p_2 = 1 - \sum_{i=3}^{d} \dot{p}_i = \dot{p}_1 + \dot{p}_2 \leqslant 1 \tag{D2}$$

and $\vec{p}_{\text{rest}} = (\dot{p}_3, \ldots, \dot{p}_d)$. One can acknowledge that two points on this line differ from each other only in the first two coordinates, hence p_1, p_2 are the only variables here. In (D2), the inequality saturates for $d = 2$ and becomes strict due to (D1) when $d > 2$.

Since we never want to move outside of the combined space, we consider only those points on the line that lie in $\boldsymbol{\omega}$. From Sec. II recall that a point of $\mathbb{R}^{2d}$ lies in Ω if and only if it meets all the requirements, (5)–(8), and if it also satisfies all the TIs, (13); only then does it belong to $\boldsymbol{\omega}$. So a point $\vec{P} = (p_1, p_2, \vec{p}_{\text{rest}}, \vec{q})$ on the line defined by (D2) is contained in Ω if and only if

$$0 \leqslant p_1 \quad \text{and} \quad 0 \leqslant p_2. \tag{D3}$$

With (D2) and (D3), one can derive

$$0 \leqslant p_1, p_2 \leqslant \dot{p}_1 + \dot{p}_2. \tag{D4}$$

As per (3) and (4), we can attach angles α_1 and α_2 to p_1 and p_2, respectively. If these angles comply with

$$\theta_{1j} - \dot{\beta}_j \leqslant \alpha_1, \quad \theta_{2k} - \dot{\beta}_k \leqslant \alpha_2 \quad \text{for all} \quad 1 \leqslant j, k \leqslant d, \tag{D5}$$

only then is $\vec{P} \in \boldsymbol{\omega}$. Observe that the other requirements for $\vec{P}$ to be in $\boldsymbol{\omega}$—(D1) for $3 \leqslant i \leqslant d$ and (7)—are automatically met, because $\vec{p}_{\text{rest}}$ and $\vec{q}$ are also parts of the interior point $(\vec{p},\vec{q}) \in \boldsymbol{\omega}$.

Considering the suprema

$$\theta_{1J} - \dot{\beta}_J = \max_{1 \leqslant j \leqslant d} \{\theta_{1j} - \dot{\beta}_j\} \quad \text{and} \tag{D6}$$

$$\theta_{2K} - \dot{\beta}_K = \max_{1 \leqslant k \leqslant d} \{\theta_{2k} - \dot{\beta}_k\}, \tag{D7}$$

we can convert all the conditions in (D5) into two:

$$\theta_{1J} - \dot{\beta}_J \leqslant \alpha_1 \quad \text{and} \quad \theta_{2K} - \dot{\beta}_K \leqslant \alpha_2. \tag{D8}$$

Throughout this paper, in the subscripts of angles, capital letters are used to highlight a supremum. A supremum, say $\theta_{1J} - \dot{\beta}_J$, cannot be a negative number: $\theta_{1J} - \dot{\beta}_J < 0$ implies $\theta_{1j} < \dot{\beta}_j$ for every j by definition (D6). This leads to $r_{1j} > \dot{q}_j$ for each j by the relations (3), (4), (9), and (10) and then to the contradiction $1 = \sum_{j=1}^{d} r_{1j} > \sum_{j=1}^{d} \dot{q}_j = 1$. Furthermore, $\theta_{1J} - \dot{\beta}_J = 0$ if and only if $\theta_{1j} = \dot{\beta}_j$ for every j. So, both suprema, (D6) and (D7), lie in $[0, \frac{\pi}{2}]$.

Since the cosine function is monotonically decreasing and nonnegative in $[0, \frac{\pi}{2}]$, we can translate the constraints, (D8), as

$$\cos\alpha_1 \leqslant \cos(\theta_{1J} - \dot{\beta}_J), \quad \cos\alpha_2 \leqslant \cos(\theta_{2K} - \dot{\beta}_K) \tag{D9}$$

and then as

$$p_1 = (\cos\alpha_1)^2 \leqslant [\cos(\theta_{1J} - \dot{\beta}_J)]^2, \tag{D10}$$

$$p_2 = (\cos\alpha_2)^2 \leqslant [\cos(\theta_{2K} - \dot{\beta}_K)]^2. \tag{D11}$$

By the way, inequalities (A17) and (A13) impose stronger restrictions than (D5), (D10), and (D11). Since p_2 follows p_1 with Eq. (D2), all the restrictions, (D4), (D10), and (D11), can be put together as

$$\begin{aligned} 0 \leqslant \max\{0\,,\, \dot{p}_1 + \dot{p}_2 - [\cos(\theta_{2K} - \dot{\beta}_K)]^2\} \leqslant p_1 \\ \leqslant \min\{[\cos(\theta_{1J} - \dot{\beta}_J)]^2,\, \dot{p}_1 + \dot{p}_2\} \leqslant 1. \end{aligned} \tag{D12}$$

One can see that these bounds on p_1 depend on the chosen interior point $(\vec{p},\vec{q})$. In short, only those $\vec{P}$ vectors that fulfill requirements (D2) and (D12) belong to the combined space $\boldsymbol{\omega}$.

From the interior point $(\vec{p},\vec{q})$, we can travel on the line in two directions: that where p_1 increases and that where p_1 decreases. When moving we pass four points $\vec{P}_1, \ldots, \vec{P}_4$ of $\mathbb{R}^{2d}$ that are presented in Table I. When we proceed in the direction where p_1 increases, then we reach either $\vec{P}_1$ or $\vec{P}_2$ first. It all depends on the minimum value in (D12). The point that we reach first belongs to $\boldsymbol{\omega}$. However, the other point fails to satisfy (D12), and thus it lies outside of $\boldsymbol{\omega}$. When moving in the other direction, where p_1 decreases, we encounter first either $\vec{P}_3$ or $\vec{P}_4$. Depending on the maximum value in (D12), one of $\{\vec{P}_3, \vec{P}_4\}$ will be inside, and the other outside, of $\boldsymbol{\omega}$ (unless both these points are the same).

All the above possibilities are listed in Table II. For any $(\vec{p},\vec{q})$, only two of these possibilities can and will materialize, thus $\boldsymbol{\omega}$ contains only a duo of (distinct) points from Table I. In Table III, we list every such duo. In fact, the interior point $(\vec{p},\vec{q})$ can be expressed as a convex combination,

$$\lambda \underbrace{(p_1', p_2', \vec{p}_{\text{rest}}, \vec{q})}_{\vec{P}'} + (1-\lambda) \underbrace{(p_1'', p_2'', \vec{p}_{\text{rest}}, \vec{q})}_{\vec{P}''}, \tag{D13}$$

of points of the one duo $\vec{P}', \vec{P}''$ that lies in $\boldsymbol{\omega}$. For each duo, $\lambda \in (0,1)$ is listed in Table III.

By varying λ from 0 to 1 in combination (D13), one can generate the line segment from $\vec{P}''$ to $\vec{P}'$. Recall that the line is described by (D2). If $\vec{P}', \vec{P}''$ belong to the combined space, then obviously the whole segment will be in $\boldsymbol{\omega}$ thanks to its

TABLE I. A list of four points $\vec{P} = (p_1, p_2, \dot{\vec{p}}_{\text{rest}}, \dot{\vec{q}}) \in \mathbb{R}^{2d}$ that lie on the line characterized by (D2). From the interior point $(\dot{\vec{p}}, \dot{\vec{q}})$, $\vec{P}_1$ and $\vec{P}_2$ are in the direction where p_1 increases, and $\vec{P}_3$ and $\vec{P}_4$ are in the direction where p_1 decreases. So, the value of p_1 for a point here is one of the four bounds [stated in (D12)]. Once we have p_1—in the middle column—then p_2 is retrieved with (D2) and listed in the right column.

$\vec{P}$	p_1	p_2
$\vec{P}_1$	$[\cos(\theta_{1J} - \dot{\beta}_J)]^2$	$\dot{p}_1 + \dot{p}_2 - [\cos(\theta_{1J} - \dot{\beta}_J)]^2$
$\vec{P}_2$	$\dot{p}_1 + \dot{p}_2$	0
$\vec{P}_3$	0	$\dot{p}_1 + \dot{p}_2$
$\vec{P}_4$	$\dot{p}_1 + \dot{p}_2 - [\cos(\theta_{2K} - \dot{\beta}_K)]^2$	$[\cos(\theta_{2K} - \dot{\beta}_K)]^2$

TABLE II. The conditions that—relying on the minimum and maximum values in (D12)—determine whether a point from Table I will be inside or outside of $\boldsymbol{\omega}$. Only if a condition listed in the left column holds does the related case in the right column occur, and vice versa. One realizes that at most two conditions can hold at a time.

If and only if	Then
$[\cos(\theta_{1J} - \dot{\beta}_J)]^2 < \dot{p}_1 + \dot{p}_2$	$\vec{P}_1 \in \boldsymbol{\omega}$ and $\vec{P}_2 \notin \boldsymbol{\omega}$
$[\cos(\theta_{1J} - \dot{\beta}_J)]^2 > \dot{p}_1 + \dot{p}_2$	$\vec{P}_1 \notin \boldsymbol{\omega}$ and $\vec{P}_2 \in \boldsymbol{\omega}$
$[\cos(\theta_{1J} - \dot{\beta}_J)]^2 = \dot{p}_1 + \dot{p}_2$	$\vec{P}_1 = \vec{P}_2 \in \boldsymbol{\omega}$
$[\cos(\theta_{2K} - \dot{\beta}_K)]^2 < \dot{p}_1 + \dot{p}_2$	$\vec{P}_3 \notin \boldsymbol{\omega}$ and $\vec{P}_4 \in \boldsymbol{\omega}$
$[\cos(\theta_{2K} - \dot{\beta}_K)]^2 > \dot{p}_1 + \dot{p}_2$	$\vec{P}_3 \in \boldsymbol{\omega}$ and $\vec{P}_4 \notin \boldsymbol{\omega}$
$[\cos(\theta_{2K} - \dot{\beta}_K)]^2 = \dot{p}_1 + \dot{p}_2$	$\vec{P}_3 = \vec{P}_4 \in \boldsymbol{\omega}$

TABLE III. Duos $\vec{P}', \vec{P}''$ of points from Table I. Only one of these duos—unless two or more duos are the same—lies in $\boldsymbol{\omega}$ and expresses the interior point $(\dot{\vec{p}}, \dot{\vec{q}})$ through the convex combination, (D13), with a real number λ. Corresponding to each duo, λ is listed in the right column. One can confirm that $0 < \lambda < 1$ by realizing $0 < \dot{p}_1 < [\cos(\theta_{1J} - \dot{\beta}_J)]^2$ and $0 < \dot{p}_2 < [\cos(\theta_{2K} - \dot{\beta}_K)]^2$.

$\vec{P}', \vec{P}''$	λ
$\vec{P}_1, \vec{P}_3$	$\dfrac{\dot{p}_1}{[\cos(\theta_{1J} - \dot{\beta}_J)]^2}$
$\vec{P}_1, \vec{P}_4$	$\dfrac{[\cos(\theta_{2K} - \dot{\beta}_K)]^2 - \dot{p}_2}{[\cos(\theta_{1J} - \dot{\beta}_J)]^2 + [\cos(\theta_{2K} - \dot{\beta}_K)]^2 - \dot{p}_1 - \dot{p}_2}$
$\vec{P}_2, \vec{P}_3$	$1 - \dfrac{\dot{p}_2}{\dot{p}_1 + \dot{p}_2}$
$\vec{P}_2, \vec{P}_4$	$1 - \dfrac{\dot{p}_2}{[\cos(\theta_{2K} - \dot{\beta}_K)]^2}$

convexity. The line segments connecting $\vec{P}_1$ to $\vec{P}_2$ (provided $\vec{P}_1 \neq \vec{P}_2$) and connecting $\vec{P}_3$ to $\vec{P}_4$ ($\vec{P}_3 \neq \vec{P}_4$) remain outside of $\boldsymbol{\omega}$. Therefore, these two duos are not listed in Table III.

Here, it is shown that every interior point $(\dot{\vec{p}}, \dot{\vec{q}})$ in $\boldsymbol{\omega}$ can be decomposed as a convex combination of *boundary* points of $\boldsymbol{\omega}$, which are decomposed in the next subsection (Appendix D 2). Note that the subsequent analysis is for $d > 2$. In the case of $d = 2$, $\dot{p}_1 + \dot{p}_2 = 1$, and Table I already includes the extreme points of $\boldsymbol{\omega}$. In fact, for $d = 2$, we only need $\vec{P}_1$ and $\vec{P}_4$, because $\boldsymbol{\omega}$ contains $\vec{P}_2$ and $\vec{P}_3$ if and only if $\vec{P}_2 = \vec{P}_1$ and $\vec{P}_3 = \vec{P}_4$, respectively.

2. Boundary of $\boldsymbol{\omega}$

The boundary of $\boldsymbol{\omega}$ is made up of $2d + d^2$ regions, where a region is characterized by equality in one of the constraints (6), (8), and (13):

$$\mathbf{P}_i := \{(\vec{p}, \vec{q}) \in \boldsymbol{\omega} \,\big|\, p_i = 0\}, \tag{D14}$$

$$\mathbf{Q}_j := \{(\vec{p}, \vec{q}) \in \boldsymbol{\omega} \,|\, q_j = 0\}, \quad \text{and} \tag{D15}$$

$$\mathbf{R}_{ij} := \{(\vec{p}, \vec{q}) \in \boldsymbol{\omega} \,|\, \alpha_i + \beta_j = \theta_{ij}\} \tag{D16}$$

for $1 \leqslant i, j \leqslant d$. A point from Table I, provided it is inside $\boldsymbol{\omega}$, is called a boundary point because it belongs to one of the regions (D14)–(D16). To reveal that the boundary points of $\boldsymbol{\omega}$ can be decomposed into certain convex combinations, let us suppose that the duo $\vec{P}_1, \vec{P}_3$ belongs to $\boldsymbol{\omega}$ and analyze first $\vec{P}_3 \in \mathbf{P}_1$ and then $\vec{P}_1 \in \mathbf{R}_{1J}$. Of course, an identical treatment can be delivered in the case of other duos in Table III.

Now we start from $\vec{P}_3$ and travel within the region $\mathbf{P}_1$ along a new set of points $\vec{P} = (0, p_2, p_3, \dot{\vec{p}}_{\text{rest}}, \dot{\vec{q}})$ by changing p_2, p_3 according to

$$p_2 + p_3 = 1 - \sum_{i=4}^{d} \dot{p}_i = \sum_{i=1}^{3} \dot{p}_i \leqslant 1, \tag{D17}$$

where $\dot{\vec{p}}_{\text{rest}} = (\dot{p}_4, \ldots, \dot{p}_d)$. Repeating the procedure, similarly to Appendix D 1, here we have

$$0 \leqslant \max\left\{0, \sum_{i=1}^{3} \dot{p}_i - [\cos(\theta_{3L} - \dot{\beta}_L)]^2\right\} \leqslant p_2$$
$$\leqslant \min\left\{[\cos(\theta_{2K} - \dot{\beta}_K)]^2, \sum_{i=1}^{3} \dot{p}_i\right\} \leqslant 1, \tag{D18}$$

which is like (D12). The supremum $\theta_{2K} - \dot{\beta}_K$ is defined by (D7) and

$$\theta_{3L} - \dot{\beta}_L = \max_{1 \leqslant l \leqslant d} \{\theta_{3l} - \dot{\beta}_l\}. \tag{D19}$$

If and only if p_2 respects (D18) and p_3 follows p_2 with (D17), then the new $\vec{P} \in \mathbf{P}_1 \subset \boldsymbol{\omega}$.

TABLE IV. A list of four points $\vec{P} = (0, p_2, p_3, \dot{\vec{p}}_{\text{rest}}, \dot{\vec{q}})$, similar to Table I. The upper bounds on p_2 [see (D18)] specify points $\vec{P}_{31}$ and $\vec{P}_{32}$, while the lower bounds determine $\vec{P}_{33}$ and $\vec{P}_{34}$. These bounds are listed in the middle column for p_2, and then the corresponding p_3 values are obtained using (D17) [see the right column].

$\vec{P}$	p_2	p_3
$\vec{P}_{31}$	$[\cos(\theta_{2K} - \dot{\beta}_K)]^2$	$\sum_{i=1}^{3} \dot{p}_i - [\cos(\theta_{2K} - \dot{\beta}_K)]^2$
$\vec{P}_{32}$	$\sum_{i=1}^{3} \dot{p}_i$	0
$\vec{P}_{33}$	0	$\sum_{i=1}^{3} \dot{p}_i$
$\vec{P}_{34}$	$\sum_{i=1}^{3} \dot{p}_i - [\cos(\theta_{3L} - \dot{\beta}_L)]^2$	$[\cos(\theta_{3L} - \dot{\beta}_L)]^2$

TABLE V. The necessary and sufficient conditions—which arise from restraint (D18)—for a point from Table IV to be inside or outside the region $\mathbf{P}_1 \subset \boldsymbol{\omega}$. This table is like Table II.

If and only if	Then
$[\cos(\theta_{2K}-\dot{\beta}_K)]^2 < \sum_{i=1}^3 \dot{p}_i$	$\vec{P}_{31} \in \mathbf{P}_1$ and $\vec{P}_{32} \notin \mathbf{P}_1$
$[\cos(\theta_{2K}-\dot{\beta}_K)]^2 > \sum_{i=1}^3 \dot{p}_i$	$\vec{P}_{31} \notin \mathbf{P}_1$ and $\vec{P}_{32} \in \mathbf{P}_1$
$[\cos(\theta_{2K}-\dot{\beta}_K)]^2 = \sum_{i=1}^3 \dot{p}_i$	$\vec{P}_{31} = \vec{P}_{32} \in \mathbf{P}_1$
$[\cos(\theta_{3L}-\dot{\beta}_L)]^2 < \sum_{i=1}^3 \dot{p}_i$	$\vec{P}_{33} \notin \mathbf{P}_1$ and $\vec{P}_{34} \in \mathbf{P}_1$
$[\cos(\theta_{3L}-\dot{\beta}_L)]^2 > \sum_{i=1}^3 \dot{p}_i$	$\vec{P}_{33} \in \mathbf{P}_1$ and $\vec{P}_{34} \notin \mathbf{P}_1$
$[\cos(\theta_{3L}-\dot{\beta}_L)]^2 = \sum_{i=1}^3 \dot{p}_i$	$\vec{P}_{33} = \vec{P}_{34} \in \mathbf{P}_1$

TABLE VI. Depending on $\vec{P}_3$ and the conditions in Table V, at most two separate points from Table IV can belong to $\mathbf{P}_1$. Here, the left column lists all such couples of points. In the right column, for each couple $\vec{P}', \vec{P}''$, the value of λ is listed, which associates the couple (provided it is within $\mathbf{P}_1$) back with $\vec{P}_3 = \lambda\vec{P}' + (1-\lambda)\vec{P}''$. Taking $0 < \dot{p}_3 < [\cos(\theta_{3L}-\dot{\beta}_L)]^2$ and $0 < \dot{p}_1 + \dot{p}_2 \leqslant [\cos(\theta_{2K}-\dot{\beta}_K)]^2$—which determines $\vec{P}_3 \in \mathbf{P}_1$ (see Table II)—one can check that each λ lies in the interval $(0,1]$.

$\vec{P}', \vec{P}''$	λ
$\vec{P}_{31}, \vec{P}_{33}$	$\dfrac{\dot{p}_1+\dot{p}_2}{[\cos(\theta_{2K}-\dot{\beta}_K)]^2}$
$\vec{P}_{31}, \vec{P}_{34}$	$\dfrac{[\cos(\theta_{3L}-\dot{\beta}_L)]^2-\dot{p}_3}{[\cos(\theta_{2K}-\dot{\beta}_K)]^2+[\cos(\theta_{3L}-\dot{\beta}_L)]^2-\sum_{i=1}^3 \dot{p}_i}$
$\vec{P}_{32}, \vec{P}_{33}$	$1-\dfrac{\dot{p}_3}{\sum_{i=1}^3 \dot{p}_i}$
$\vec{P}_{32}, \vec{P}_{34}$	$1-\dfrac{\dot{p}_3}{[\cos(\theta_{3L}-\dot{\beta}_L)]^2}$

Analogously to Tables I–III, here we present Tables IV–VI, in that order. Table IV reports a collection of four points. Table V lists the conditions that determine whether a point from Table IV is inside or outside $\mathbf{P}_1$. Table VI reports all possible couples of points from Table IV one of which belongs to $\mathbf{P}_1$; that one is determined by $\vec{P}_3$. The line segment connecting the one couple carries $\vec{P}_3$ and is located completely within region $\mathbf{P}_1$.

Now we focus on $\vec{P}_1 \in \mathbf{R}_{1J}$. Let us proceed from $\vec{P}_1$ by altering only p_2, p_3 of another new vector, $\vec{P} = ([\cos(\theta_{1J}-\dot{\beta}_J)]^2, p_2, p_3, \dot{\vec{p}}_{\text{rest}}, \dot{\vec{q}})$, with respect to

$$p_2 + p_3 = 1 - \sum_{i=4}^{d} \dot{p}_i - [\cos(\theta_{1J}-\dot{\beta}_J)]^2 = \sum_{i=1}^{3} \dot{p}_i - [\cos(\theta_{1J}-\dot{\beta}_J)]^2. \tag{D20}$$

Note that $\dot{\vec{p}}_{\text{rest}} = (\dot{p}_4, \ldots, \dot{p}_d)$, and (D20) identifies a straight line, a segment of which is contained in the region $\mathbf{R}_{1J}$. In addition to (D20), if p_2 agrees with

$$\begin{aligned} &0 \\ &\leqslant \max\left\{0\,, \sum_{i=1}^{3} \dot{p}_i - [\cos(\theta_{1J}-\dot{\beta}_J)]^2 - [\cos(\theta_{3L}-\dot{\beta}_L)]^2\right\} \\ &\leqslant p_2 \\ &\leqslant \min\left\{[\cos(\theta_{2K}-\dot{\beta}_K)]^2, \sum_{i=1}^{3} \dot{p}_i - [\cos(\theta_{1J}-\dot{\beta}_J)]^2\right\} \\ &\leqslant 1, \end{aligned} \tag{D21}$$

only then is the new vector $\vec{P} \in \mathbf{R}_{1J}$. Like Tables I and IV, here we construct Table VII of four points using the four bounds in (D21).

Due to (C4) and (C7) from Appendix C, we have the following:

$$\text{if} \quad K \neq J, \quad \text{then}$$
$$1 < [\cos(\theta_{1J}-\dot{\beta}_J)]^2 + [\cos(\theta_{2K}-\dot{\beta}_K)]^2, \quad \text{and} \tag{D22}$$
$$\text{if} \quad L \neq J, \quad \text{then}$$
$$1 < [\cos(\theta_{1J}-\dot{\beta}_J)]^2 + [\cos(\theta_{3L}-\dot{\beta}_L)]^2. \tag{D23}$$

These inequalities are strict because a requirement in (C7), $\dot{\beta}_J + \dot{\beta}_K = \frac{\pi}{2}$, cannot be met since $\dot{q}_J + \dot{q}_K < 1$ is caused by (D1). Now taking (D21)–(D23) with $\sum_{i=1}^3 \dot{p}_i \leqslant 1$, one can deduce that the vectors $\vec{P}_{11}$ and $\vec{P}_{14}$ in Table VII cannot belong to $\mathbf{R}_{1J}$ unless $K = J$ and $L = J$, respectively. This fact is reported in Table VIII with some other conditions; together they tell when a point from Table VII will be inside or outside region $\mathbf{R}_{1J}$.

A duo, of the four listed in Table IX, resides in $\mathbf{R}_{1J}$ and expresses $\vec{P}_1$ through a convex combination. As Tables I–III are linked with the interior point $(\vec{p}, \dot{\vec{q}}) \in \boldsymbol{\omega}$ and Tables IV–VI are attached to $\vec{P}_3 \in \mathbf{P}_1$, Tables VII–IX are associated with $\vec{P}_1 \in \mathbf{R}_{1J}$. Tables I, IV, and VII incude the boundary points of $\boldsymbol{\omega}$, $\mathbf{P}_1$, and $\mathbf{R}_{1J}$, respectively.

TABLE VII. A set of four points $\vec{P} = ([\cos(\theta_{1J}-\dot{\beta}_J)]^2, p_2, p_3, \dot{\vec{p}}_{\text{rest}}, \dot{\vec{q}})$, like Tables I and IV. Here $\{\vec{P}_{11}, \vec{P}_{12}\}$ and $\{\vec{P}_{13}, \vec{P}_{14}\}$ are obtained with the upper and lower bounds in (D21), respectively. These bounds are listed in the middle column, and p_3 is obtained from p_2 using (D20).

$\vec{P}$	p_2	p_3
$\vec{P}_{11}$	$[\cos(\theta_{2K}-\dot{\beta}_K)]^2$	$\sum_{i=1}^3 \dot{p}_i - [\cos(\theta_{1J}-\dot{\beta}_J)]^2 - [\cos(\theta_{2K}-\dot{\beta}_K)]^2$
$\vec{P}_{12}$	$\sum_{i=1}^3 \dot{p}_i - [\cos(\theta_{1J}-\dot{\beta}_J)]^2$	0
$\vec{P}_{13}$	0	$\sum_{i=1}^3 \dot{p}_i - [\cos(\theta_{1J}-\dot{\beta}_J)]^2$
$\vec{P}_{14}$	$\sum_{i=1}^3 \dot{p}_i - [\cos(\theta_{1J}-\dot{\beta}_J)]^2 - [\cos(\theta_{3L}-\dot{\beta}_L)]^2$	$[\cos(\theta_{3L}-\dot{\beta}_L)]^2$

TABLE VIII. Where there is a case from the left column, we list the corresponding consequence in the right column. All these cases are implications of (D21)–(D23). The table is constructed in the same way as Tables II and V.

	If	Then
$K \neq J$		$\vec{P}_{11} \notin \mathbf{R}_{1J}$ and $\vec{P}_{12} \in \mathbf{R}_{1J}$
	$[\cos(\theta_{1J} - \dot{\beta}_J)]^2 + [\cos(\theta_{2K} - \dot{\beta}_K)]^2 < \sum_{i=1}^3 \dot{p}_i$	$\vec{P}_{11} \in \mathbf{R}_{1J}$ and $\vec{P}_{12} \notin \mathbf{R}_{1J}$
$K = J$ and	$[\cos(\theta_{1J} - \dot{\beta}_J)]^2 + [\cos(\theta_{2K} - \dot{\beta}_K)]^2 > \sum_{i=1}^3 \dot{p}_i$	$\vec{P}_{11} \notin \mathbf{R}_{1J}$ and $\vec{P}_{12} \in \mathbf{R}_{1J}$
	$[\cos(\theta_{1J} - \dot{\beta}_J)]^2 + [\cos(\theta_{2K} - \dot{\beta}_K)]^2 = \sum_{i=1}^3 \dot{p}_i$	$\vec{P}_{11} = \vec{P}_{12} \in \mathbf{R}_{1J}$
$L \neq J$		$\vec{P}_{13} \in \mathbf{R}_{1J}$ and $\vec{P}_{14} \notin \mathbf{R}_{1J}$
	$[\cos(\theta_{1J} - \dot{\beta}_J)]^2 + [\cos(\theta_{3L} - \dot{\beta}_L)]^2 < \sum_{i=1}^3 \dot{p}_i$	$\vec{P}_{13} \notin \mathbf{R}_{1J}$ and $\vec{P}_{14} \in \mathbf{R}_{1J}$
$L = J$ and	$[\cos(\theta_{1J} - \dot{\beta}_J)]^2 + [\cos(\theta_{3L} - \dot{\beta}_L)]^2 > \sum_{i=1}^3 \dot{p}_i$	$\vec{P}_{13} \in \mathbf{R}_{1J}$ and $\vec{P}_{14} \notin \mathbf{R}_{1J}$
	$[\cos(\theta_{1J} - \dot{\beta}_J)]^2 + [\cos(\theta_{3L} - \dot{\beta}_L)]^2 = \sum_{i=1}^3 \dot{p}_i$	$\vec{P}_{13} = \vec{P}_{14} \in \mathbf{R}_{1J}$

TABLE IX. Taking the case $K = J$ and $L = J$, we have four duos of points, and the table is arranged in the same manner as Tables III and VI. In the right column, we list the λ value that relates the duo (when it is in $\mathbf{R}_{1J}$) to the point $\vec{P}_1 = \lambda\vec{P}' + (1-\lambda)\vec{P}''$. Having $0 < \dot{p}_i < [\cos(\theta_{iJ} - \dot{\beta}_J)]^2$ for $i = 1,2,3$ and the condition $[\cos(\theta_{1J} - \dot{\beta}_J)]^2 \leqslant \dot{p}_1 + \dot{p}_2$, which ensures that $\vec{P}_1 \in \mathbf{R}_{1J}$ (see Table II), one can show that $0 \leqslant \lambda < 1$ in every case.

$\vec{P}', \vec{P}''$	λ
$\vec{P}_{11}, \vec{P}_{13}$	$\dfrac{\dot{p}_1 + \dot{p}_2 - [\cos(\theta_{1J} - \dot{\beta}_J)]^2}{[\cos(\theta_{2J} - \dot{\beta}_J)]^2}$
$\vec{P}_{11}, \vec{P}_{14}$	$\dfrac{[\cos(\theta_{3J} - \dot{\beta}_J)]^2 - \dot{p}_3}{\sum_{i=1}^3 \{[\cos(\theta_{iJ} - \dot{\beta}_J)]^2 - \dot{p}_i\}}$
$\vec{P}_{12}, \vec{P}_{13}$	$1 - \dfrac{\dot{p}_3}{\sum_{i=1}^3 \dot{p}_i - [\cos(\theta_{1J} - \dot{\beta}_J)]^2}$
$\vec{P}_{12}, \vec{P}_{14}$	$1 - \dfrac{\dot{p}_3}{[\cos(\theta_{3J} - \dot{\beta}_J)]^2}$

3. Extreme of $\boldsymbol{\omega}$

In the above subsections, it is demonstrated that every interior point $(\dot{\vec{p}}, \dot{\vec{q}}) \in \boldsymbol{\omega}$ can be decomposed into a convex combination of the boundary points of $\boldsymbol{\omega}$, which can further be decomposed into convex combinations of the boundary points of regions (D14)–(D16). Continuing this decomposition process, we reach a point $(\mathring{\dot{\vec{p}}}, \dot{\vec{q}})$, where

$$\mathring{\dot{\vec{p}}} = ((\cos\mathring{\alpha}_1)^2, \ldots, (\cos\mathring{\alpha}_m)^2, \mathbf{0}, \mathring{p}_s, \mathbf{0}), \tag{D24}$$

$$\mathring{\alpha}_i = \theta_{iJ} - \dot{\beta}_J \quad (\text{for all} \quad i = 1, \ldots, m), \tag{D25}$$

$$\mathring{p}_s = 1 - \sum_{i=1}^{m} (\cos\mathring{\alpha}_i)^2 \quad (m+1 \leqslant s \leqslant d), \tag{D26}$$

$$\mathbf{0} \equiv 0, \ldots, 0, \quad \text{and} \tag{D27}$$

$$1 \leqslant m \leqslant d - 1. \tag{D28}$$

Since every $\mathring{\alpha}_i$ of (D25) is a supremum, $0 \leqslant \mathring{\alpha}_i$ [see the explanation following (D8)] and $\mathring{\alpha}_i < \dot{\alpha}_i < \frac{\pi}{2}$ due to (D1), we deduce that

$$0 \leqslant \mathring{\alpha}_i < \frac{\pi}{2} \quad (\text{for all} \quad i = 1, \ldots, m). \tag{D29}$$

The point $(\mathring{\dot{\vec{p}}}, \dot{\vec{q}})$, determined by (D24)–(D28), satisfies m and $d - (m+1)$ number of *equality* constraints of types (13) and (6), respectively. If $\mathring{p}_s$ of (D26) follows

$$0 \leqslant \mathring{p}_s \leqslant [\cos(\theta_{sZ} - \dot{\beta}_Z)]^2, \tag{D30}$$

then $(\mathring{\dot{\vec{p}}}, \dot{\vec{q}}) \in \boldsymbol{\omega}$, where

$$\theta_{sZ} - \dot{\beta}_Z = \max_{1 \leqslant z \leqslant d} \{\theta_{sz} - \dot{\beta}_z\} \tag{D31}$$

is a supremum like (D6), (D7), (D19), and (D25). One can check that points in Table I for $d = 2$ and in Tables IV as well as VII—provided $K = J$ and $L = J$—for $d = 3$ are like $(\mathring{\dot{\vec{p}}}, \dot{\vec{q}})$; remember that $\sum_{i=1}^{d} \dot{p}_i = 1$ due to (5). Furthermore, one can easily recognize $\mathring{p}_s$ in each of these points. Then one can see through Tables II, V, and VIII that one of the two inequalities in (D30) is required for a point to be inside $\boldsymbol{\omega}$. The other inequality is automatically obeyed due to (D1) and the conditions appearing in the earlier decompositions.

If we start our journey from a point $(\dot{\vec{p}}, \dot{\vec{q}})$, where

$$\dot{\vec{q}} = (r_{11}, \ldots, r_{1d}), \tag{D32}$$

then we will arrive at the point $(\mathring{\dot{\vec{p}}}, \dot{\vec{q}})$, where

$$\mathring{\dot{\vec{p}}} = (1, \mathbf{0}) \tag{D33}$$

[for $\mathbf{0}$, see (D27)]. This point represents an extreme point in $\boldsymbol{\omega}$ and a special case,

$$m = 1 \quad \text{with} \quad 0 = \mathring{p}_s, \tag{D34}$$

of (D28) and (D26). In the case (D34), the supremum $\mathring{\alpha}_1 = \theta_{1J} - \dot{\beta}_J = 0$, which is possible if and only if $\theta_{1j} = \dot{\beta}_j$, means that $r_{1j} = \dot{q}_j$, for every j. Indeed, this is so [see (D32)]. In all other cases, $0 < \mathring{\alpha}_i$ for every $1 \leqslant i \leqslant m$ [see the limits (D29) on $\mathring{\alpha}_i$ of (D25)], and $(\mathring{\dot{\vec{p}}}, \dot{\vec{q}})$ can be decomposed further by adopting the same procedure as before.

Without loss of generality, let us suppose $J = 1$ for the subsequent analysis. Here we begin with $\vec{Q} = (\mathring{\dot{\vec{p}}}, \dot{q}_1, q_2, q_3, \dot{\vec{q}}_{\text{rest}})$,

where

$$q_2 + q_3 = 1 - \sum_{i=4}^{d} \dot{q}_j - \underbrace{(\cos\dot{\beta}_1)^2}_{\dot{q}_1} = \dot{q}_2 + \dot{q}_3 \tag{D35}$$

and $\dot{\vec{q}}_{\text{rest}} = (\dot{q}_4, \ldots, \dot{q}_d)$. One can acknowledge that $\vec{Q}$ represents all those points, including $(\mathring{\vec{p}}\,, \dot{\vec{q}})$, that fall on the straight line characterized by (D35).

If q_3 stays on the line with q_2, which follows

$$\begin{aligned} 0 \leqslant \max\{0\,, \dot{q}_2 + \dot{q}_3 - [\cos(\theta_{L3} - \mathring{\alpha}_L)]^2\} \leqslant q_2 \\ \leqslant \min\{[\cos(\theta_{K2} - \mathring{\alpha}_K)]^2, \dot{q}_2 + \dot{q}_3\} \leqslant 1, \end{aligned} \tag{D36}$$

then $\vec{Q} \in \boldsymbol{\omega}$. Here

$$\theta_{K2} - \mathring{\alpha}_K = \max_{1\leqslant k\leqslant d} \{\theta_{k2} - \mathring{\alpha}_k\} \quad \text{and} \tag{D37}$$

$$\theta_{L3} - \mathring{\alpha}_L = \max_{1\leqslant l\leqslant d} \{\theta_{l3} - \mathring{\alpha}_l\} \tag{D38}$$

are suprema, and the angles $\mathring{\alpha}$ are related to the components of $\mathring{\vec{p}}$ through (3) and (4) [see also (D24) and (D25)]. Constraints (D36) look like (D12) and (D18). Identically to Tables I, IV, and VII, we list four points in Table X, which are drawn from the four bounds on q_2 given in (D36).

Now, to establish the criteria for a point from Table X to be inside or outside $\boldsymbol{\omega}$, we address the two cases

$$m = 1 \quad \text{with} \quad 0 < \mathring{p}_s \quad \text{and} \tag{D39}$$

$$m > 1 \quad \text{with} \quad 0 < \mathring{p}_s \tag{D40}$$

individually [see Eq. (D26) for $\mathring{p}_s$ and the range, (D28), of m]. Let us first take the case (D40): whatever the suprema (D37) and (D38) are, we have

$$1 < (\cos\dot{\beta}_1)^2 + [\cos(\theta_{K2} - \mathring{\alpha}_K)]^2 \quad \text{and} \tag{D41}$$

$$1 < (\cos\dot{\beta}_1)^2 + [\cos(\theta_{L3} - \mathring{\alpha}_L)]^2. \tag{D42}$$

To demonstrate this, we consider $m = 2$; cases with $m > 2$ can be handled likewise. For $m = 2$, we have $\dot{\beta}_1 = \theta_{i1} - \mathring{\alpha}_i$ (where $i = 1,2$) due to (D25). If K associated with supremum (D37) is 1, then by taking $\dot{\beta}_1 = \theta_{21} - \mathring{\alpha}_2$ we can validate the strict inequality, (D41), thanks to (C9). If $K \neq 1$, we can do the same by now considering $\dot{\beta}_1 = \theta_{11} - \mathring{\alpha}_1$. In a similar fashion, we can establish the other inequality, (D42).

TABLE X. Four points $\vec{Q} = (\mathring{\vec{p}}, \dot{q}_1, q_2, q_3, \dot{\vec{q}}_{\text{rest}}) \in \mathbb{R}^{2d}$ that rest on the line specified by (D35). From point $(\mathring{\vec{p}}\,, \dot{\vec{q}})$, the coordinate q_2 increases towards $\{\vec{Q}_1, \vec{Q}_2\}$, while it decreases towards $\{\vec{Q}_3, \vec{Q}_4\}$. The middle column lists the four bounds given in (D36), and then q_3 is obtained with (D35) and listed in the right column. The table is constructed in the same fashion as Tables I, IV, and VII.

$\vec{Q}$	q_2	q_3
$\vec{Q}_1$	$[\cos(\theta_{K2} - \mathring{\alpha}_K)]^2$	$\dot{q}_2 + \dot{q}_3 - [\cos(\theta_{K2} - \mathring{\alpha}_K)]^2$
$\vec{Q}_2$	$\dot{q}_2 + \dot{q}_3$	0
$\vec{Q}_3$	0	$\dot{q}_2 + \dot{q}_3$
$\vec{Q}_4$	$\dot{q}_2 + \dot{q}_3 - [\cos(\theta_{L3} - \mathring{\alpha}_L)]^2$	$[\cos(\theta_{L3} - \mathring{\alpha}_L)]^2$

We draw the following inferences from inequalities (D41) and (D42):

$$[\cos(\theta_{K2} - \mathring{\alpha}_K)]^2 > 1 - \dot{q}_1 = \sum_{j=2}^{d} \dot{q}_j \geqslant \dot{q}_2 + \dot{q}_3, \tag{D43}$$

$$[\cos(\theta_{L3} - \mathring{\alpha}_L)]^2 > 1 - \dot{q}_1 = \sum_{j=2}^{d} \dot{q}_j \geqslant \dot{q}_2 + \dot{q}_3, \tag{D44}$$

which imply that the maximum and the minimum values in (D36) are 0 and $\dot{q}_2 + \dot{q}_3$, respectively. Consequently, points $\vec{Q}_1$ and $\vec{Q}_4$ in Table X never belong to $\boldsymbol{\omega}$ in the case (D40), whereas $\vec{Q}_2$ and $\vec{Q}_3$ always do. Moreover, $(\mathring{\vec{p}}\,, \dot{\vec{q}})$ can be broken into the convex combination $\lambda\,\vec{Q}_2 + (1-\lambda)\,\vec{Q}_3$, where $\lambda = \frac{\dot{q}_2}{\dot{q}_2+\dot{q}_3}$ (see Table XII).

Next, it is not difficult to realize that both $\vec{Q}_2$ and $\vec{Q}_3$ can be decomposed further and further until we arrive at a point $(\mathring{\vec{p}}\,, \mathring{\vec{q}})$, where

$$\mathring{\vec{q}} = (\dot{q}_1, \mathbf{0}, \mathring{q}_t, \mathbf{0}) \quad \text{with} \quad \mathring{q}_t = 1 - \dot{q}_1 \quad (2 \leqslant t \leqslant d). \tag{D45}$$

In the decomposition process one will encounter inequalities, such as (D41) and (D42), that can be tacked like the above. For $m > 1$, a point $(\mathring{\vec{p}}\,, \mathring{\vec{q}})$ defined by (D24)–(D27) and (D45) is an extreme point of $\boldsymbol{\omega}$, because it cannot be written into a convex combination of other points of $\boldsymbol{\omega}$. Furthermore, $(\mathring{\vec{p}}\,, \mathring{\vec{q}})$ is a vector-valued function of $\dot{\beta}_1$ since θ angles are fixed by (10) once the measurement settings are selected in (1).

Let us now turn to the case (D39), where $\dot{\beta}_1 = \theta_{11} - \mathring{\alpha}_1$ according to (D25),

$$\vec{Q} = (\mathring{\vec{p}}, [\cos(\theta_{11} - \mathring{\alpha}_1)]^2, q_2, q_3, \dot{\vec{q}}_{\text{rest}}), \quad \text{and} \tag{D46}$$

$$\mathring{\vec{p}} = (\mathring{p}_1, \mathbf{0}, \mathring{p}_s, \mathbf{0}), \quad \text{with} \quad 1 - \mathring{p}_s = \mathring{p}_1 = (\cos\mathring{\alpha}_1)^2. \tag{D47}$$

Since supremum (D37) is a nonnegative number, K can be either s or 1 here. This is because $\theta_{i2} - \mathring{\alpha}_i \leqslant 0$ when $i \neq s$ and $i \neq 1$, as then $\mathring{\alpha}_i = \frac{\pi}{2}$ and every $\theta \leqslant \frac{\pi}{2}$. Similarly, L related to supremum (D38) can be either s or 1 here.

When $K = s$ or $L = s$ or both, we encounter a situation similar to the case (D40): When $K = s$, then, due to (C9), we have

$$[\cos(\theta_{K2} - \mathring{\alpha}_K)]^2 + [\cos(\theta_{11} - \mathring{\alpha}_1)]^2 \geqslant 1 \quad \text{and thus} \tag{D48}$$

$$[\cos(\theta_{K2} - \mathring{\alpha}_K)]^2 \geqslant 1 - \dot{q}_1 = \sum_{j=2}^{d} \dot{q}_j \geqslant \dot{q}_2 + \dot{q}_3. \tag{D49}$$

One can see that (D48) and (D49) are analogous to (D41) and (D43), respectively. The inequalities in (D49) suggest that $\dot{q}_2 + \dot{q}_3$ is the minimum value in (D36). Therefore, without exception $\vec{Q}_2$ lies within $\boldsymbol{\omega}$; if $\vec{Q}_1 = \vec{Q}_2$, then $\vec{Q}_1 \in \boldsymbol{\omega}$. Identically, for $L = s$, always $\vec{Q}_3 \in \boldsymbol{\omega}$, and $\vec{Q}_4$ belongs to $\boldsymbol{\omega}$ only when it is $\vec{Q}_3$.

Only when $K = 1$ and $L = 1$ can $\vec{Q}_1$ and $\vec{Q}_4$ be inside $\boldsymbol{\omega}$ without being equal to $\vec{Q}_2$ and $\vec{Q}_3$, respectively (see Table XI). With Table XI, for the case (D39), one can determine whether or not a duplet of points from Table X lies within $\boldsymbol{\omega}$.

TABLE XI. Group of conditions for the case (D39), where $\mathring{\alpha}_1 = \theta_{11} - \dot{\beta}_1$. The condition listed in the left column provides the entry in the right column. These conditions originate from (D36) and the discussion around (D49). At most two conditions can hold simultaneously, thus more than two distinct points from Table X cannot be a part of $\boldsymbol{\omega}$. This table looks like Table VIII.

	If	Then
$K = s$		$\vec{Q}_2 \in \boldsymbol{\omega}$
	$[\cos(\theta_{K2} - \mathring{\alpha}_K)]^2 < \dot{q}_2 + \dot{q}_3$	$\vec{Q}_1 \in \boldsymbol{\omega}$ and $\vec{Q}_2 \notin \boldsymbol{\omega}$
$K = 1$,	$[\cos(\theta_{K2} - \mathring{\alpha}_K)]^2 > \dot{q}_2 + \dot{q}_3$	$\vec{Q}_1 \notin \boldsymbol{\omega}$ and $\vec{Q}_2 \in \boldsymbol{\omega}$
	$[\cos(\theta_{K2} - \mathring{\alpha}_K)]^2 = \dot{q}_2 + \dot{q}_3$	$\vec{Q}_1 = \vec{Q}_2 \in \boldsymbol{\omega}$
$L = s$		$\vec{Q}_3 \in \boldsymbol{\omega}$
	$[\cos(\theta_{L3} - \mathring{\alpha}_L)]^2 < \dot{q}_2 + \dot{q}_3$	$\vec{Q}_3 \notin \boldsymbol{\omega}$ and $\vec{Q}_4 \in \boldsymbol{\omega}$
$L = 1$,	$[\cos(\theta_{L3} - \mathring{\alpha}_L)]^2 > \dot{q}_2 + \dot{q}_3$	$\vec{Q}_3 \in \boldsymbol{\omega}$ and $\vec{Q}_4 \notin \boldsymbol{\omega}$
	$[\cos(\theta_{L3} - \mathring{\alpha}_L)]^2 = \dot{q}_2 + \dot{q}_3$	$\vec{Q}_3 = \vec{Q}_4 \in \boldsymbol{\omega}$

TABLE XII. Collection of duplets $\vec{Q}', \vec{Q}''$ of points from Table X. Only one of these duplets—unless two or more are the same—belongs to $\boldsymbol{\omega}$ and represents point $(\mathring{\vec{p}}, \mathring{\vec{q}})$ with the convex combination $\lambda\,\vec{Q}' + (1-\lambda)\,\vec{Q}''$. Here we assume that $K = 1$ and $L = 1$; otherwise, $\vec{Q}_1$ and $\vec{Q}_4$ cannot belong to $\boldsymbol{\omega}$ without being equal to $\vec{Q}_2$ and $\vec{Q}_3$, respectively (see Table XI). The right column lists the values of λ for each duplet, provided the duplet lies within $\boldsymbol{\omega}$. One can check that $\lambda \in [0,1]$ with $0 < \dot{q}_2 \leqslant [\cos(\theta_{K2} - \mathring{\alpha}_K)]^2$ and $0 < \dot{q}_3 \leqslant [\cos(\theta_{L3} - \mathring{\alpha}_L)]^2$ [see (D36)].

$\vec{Q}', \vec{Q}''$	λ
$\vec{Q}_1, \vec{Q}_3$	$\dfrac{\dot{q}_2}{[\cos(\theta_{12} - \mathring{\alpha}_1)]^2}$
$\vec{Q}_1, \vec{Q}_4$	$\dfrac{[\cos(\theta_{13} - \mathring{\alpha}_1)]^2 - \dot{q}_3}{[\cos(\theta_{12} - \mathring{\alpha}_1)]^2 + [\cos(\theta_{13} - \mathring{\alpha}_1)]^2 - \dot{q}_2 - \dot{q}_3}$
$\vec{Q}_2, \vec{Q}_3$	$1 - \dfrac{\dot{q}_3}{\dot{q}_2 + \dot{q}_3}$
$\vec{Q}_2, \vec{Q}_4$	$1 - \dfrac{\dot{q}_3}{[\cos(\theta_{13} - \mathring{\alpha}_1)]^2}$

All such duplets are listed in Table XII, which reveals that point $(\mathring{\vec{p}}, \mathring{\vec{q}})$ can be split into a convex combination. As before, we can break the points in Table X further and further until we reach extreme points of $\boldsymbol{\omega}$.

In the case (D39), the decomposition process leads to

$$\mathring{\vec{q}} = ((\cos\mathring{\beta}_1)^2, \ldots, (\cos\mathring{\beta}_n)^2, \mathbf{0}, \mathring{q}_t, \mathbf{0}), \quad \text{where} \tag{D50}$$

$$\mathring{\beta}_j = \theta_{1j} - \mathring{\alpha}_1 \quad (\text{for all} \quad j = 1, \ldots, n), \tag{D51}$$

$$\mathring{q}_t = 1 - \sum_{j=1}^{n} (\cos\mathring{\beta}_j)^2 \quad (n+1 \leqslant t \leqslant d), \quad \text{and} \tag{D52}$$

$$1 \leqslant n \leqslant d-1. \tag{D53}$$

If $\mathring{q}_t$ of (D52) obeys

$$0 \leqslant \mathring{q}_t \leqslant [\cos(\theta_{Zt} - \mathring{\alpha}_Z)]^2, \quad \text{where} \tag{D54}$$

$$\theta_{Zt} - \mathring{\alpha}_Z = \max_{1 \leqslant z \leqslant d} \{\theta_{zt} - \mathring{\alpha}_z\}, \tag{D55}$$

then point $(\mathring{\vec{p}}, \mathring{\vec{q}})$, provided by (D47) and (D50), belongs to $\boldsymbol{\omega}$. It is an extreme point of $\boldsymbol{\omega}$ in the case (D39). One also realizes that both $\mathring{\vec{p}}$ and $\mathring{\vec{q}}$ are functions of $\dot{\beta}_1$ by noting that $\mathring{\beta}_j = \theta_{1j} - \theta_{11} + \dot{\beta}_1$ in (D51) with $\mathring{\alpha}_1 = \theta_{11} - \dot{\beta}_1$. In fact, the extreme point identified by (D33) and (D32) in the case (D34) can also be represented by the $\mathring{\vec{p}}$ and $\mathring{\vec{q}}$ of (D47) and (D50) by taking $\mathring{\alpha}_1 = 0$, which makes it an endpoint of the parametric curve $(\mathring{\vec{p}}_{(\mathring{\alpha}_1)}, \mathring{\vec{q}}_{(\mathring{\alpha}_1)})$. In conclusion, we realize the *structure* of extreme points of $\boldsymbol{\omega}$:

The point $(\mathring{\vec{p}}, \mathring{\vec{q}}\,)$, where "$\mathring{\vec{p}}$ is specified by (D24)–(D27) and $\mathring{\vec{q}}$ is given by (D45)" when $m > 1$ and "$\mathring{\vec{p}}$ is described by (D47) and $\mathring{\vec{q}}$ is presented by (D50)–(D53)" when $m = 1$, represents an extreme point of $\boldsymbol{\omega}$ provided $\dot{\beta}_1$ is within suitable limits presented in the next subsection (Appendix D 4). For every $1 \leqslant m \leqslant (d-1)$, $(\mathring{\vec{p}}_{(\dot{\beta}_1)}, \mathring{\vec{q}}_{(\dot{\beta}_1)})$ is a vector-valued function of a real parameter $\dot{\beta}_1$, thus it characterizes an m-parametric curve in $\boldsymbol{\omega}$. Such curves are presented in Sec. II. (D56)

4. Limits on β_1

We start with the m-parametric curve $(\vec{p}_{(\beta_1)}, \vec{q}_{(\beta_1)})$ identified by (16)–(21). According to (D56), a part of the curve that lies within $\boldsymbol{\omega}$ represents its extreme points. This part is specified by the upper and lower limits of β_1. To compute these limits, here, we need to consider only

$$0 \leqslant p_s, \tag{D57}$$

$$\theta_{it} \leqslant \alpha_i + \beta_t \quad (\text{for} \quad i = 1, \ldots, m, s), \quad \text{and} \tag{D58}$$

$$\theta_{sj} \leqslant \alpha_s + \beta_j \quad (\text{for} \quad j = 1, t). \tag{D59}$$

When $i > m$ and $i \neq s$, then $\alpha_i = \frac{\pi}{2}$, and when $j \neq 1$ and $j \neq t$, then $\beta_j = \frac{\pi}{2}$. So one can easily perceive that points $(\vec{p}_{(\beta_1)}, \vec{q}_{(\beta_1)})$ fulfill the rest of the requirements, (13) as well as (5)–(8), to be inside $\boldsymbol{\omega}$.

For $i = s$ in (D58) or $j = t$ in (D59), the TI is always obeyed: due to

$$\frac{\pi}{2} \leqslant \alpha_s + \alpha_1 \tag{D60}$$

$$= \alpha_s + \theta_{11} - \beta_1 \tag{D61}$$

$$= \alpha_s + \theta_{11} - \frac{\pi}{2} + \beta_t, \tag{D62}$$

we have

$$\frac{\pi}{2} \leqslant \pi - \theta_{11} \leqslant \alpha_s + \beta_t. \tag{D63}$$

With (C8), (16), and (C3) one can sequentially go through steps (D60)–(D62), and the left-hand-side inequality in (D63) is a consequence of $\theta \leqslant \frac{\pi}{2}$. Since α_s and β_t obey $\frac{\pi}{2} \leqslant \alpha_s + \beta_t$, they certainly follow the TI $\theta_{st} \leqslant \alpha_s + \beta_t$ as every $\theta \leqslant \frac{\pi}{2}$.

If we decrease β_1, then $\alpha_s + \beta_1$ decreases, and β_1 reaches its lower limit β' when inequality (D59), for $j = 1$, becomes saturated. This means that β' is a solution of the equation

$\theta_{s1} - \beta' = \alpha_s$ and thus of

$$[\cos(\theta_{s1} - \beta')]^2 = p_s = 1 - \sum_{i=1}^{m} [\cos(\theta_{i1} - \beta')]^2 \quad \text{(D64)}$$

[by (16) and (19)]. If we increase β_1, then p_s and $\alpha_i + \beta_t$ $(i = 1, \ldots, m)$ decrease, and β_1 attains its upper limit β'' as soon as one of the inequalities (D57) and (D58) becomes saturated. Using (16), (19), and $\beta_t = \frac{\pi}{2} - \beta_1$ [owing to (C3)], these inequalities can be expressed as

$$0 \leqslant 1 - \sum_{i=1}^{m} [\cos(\theta_{i1} - \beta_1)]^2 \quad \text{and} \quad \text{(D65)}$$

$$\beta_1 \leqslant \frac{\theta_{i1} - \theta_{it}}{2} + \frac{\pi}{4} \quad (\text{for } i = 1, \ldots, m). \quad \text{(D66)}$$

Now we need to investigate the two cases $m = 1$ and $1 < m \leqslant (d-1)$, listed in (D56), separately for β''.

In the case $m = 1$, (D65) clearly holds, and the upper limit

$$\beta'' = \frac{\theta_{11} - \theta_{1t}}{2} + \frac{\pi}{4} \quad \text{(D67)}$$

is obtained when (D66) is saturated. Corresponding to β'' of (D67), we have

$$\alpha_1 = \theta_{11} - \beta'' = \frac{\theta_{11} + \theta_{1t}}{2} - \frac{\pi}{4}, \quad \text{(D68)}$$

which is a root of the equation

$$[\cos(\theta_{11} - \alpha_1)]^2 + [\cos(\theta_{1t} - \alpha_1)]^2 = 1. \quad \text{(D69)}$$

In the case $1 < m \leqslant (d-1)$, when we increase β_1, then inequality (D65), rather than (D66), becomes saturated first. Hence, β'' is now a solution of

$$\sum_{i=1}^{m} [\cos(\theta_{i1} - \beta'')]^2 = 1. \quad \text{(D70)}$$

One can justify these statements by proving that

$$\beta'' \leqslant \underbrace{\frac{\theta_{i1} + \theta_{i'1}}{2} - \frac{\pi}{4}}_{\widetilde{\beta}} \leqslant \frac{\theta_{i1} - \theta_{it}}{2} + \frac{\pi}{4}, \quad \text{(D71)}$$

where $1 \leqslant i, i' \leqslant m$. As β'' is a root of Eq. (D70), $\widetilde{\beta}$ is a root of

$$[\cos(\theta_{i1} - \widetilde{\beta})]^2 + [\cos(\theta_{i'1} - \widetilde{\beta})]^2 = 1. \quad \text{(D72)}$$

Equations (D64), (D70), and (D72) are of the form

$$\sum_{i=1}^{\mathrm{M}} [\cos(\theta_{i1} - \beta_1)]^2 = 1, \quad \text{(D73)}$$

where M angles—the M set $\{\theta_{11}, \ldots, \theta_{\mathrm{M}1}\}$—are taken from the first column in the Θ matrix [given in (11)]. Always, we must choose the root of Eq. (D73) that respects $0 \leqslant \beta_1 \leqslant \theta_{i1}$ for every $i = 1, \ldots, \mathrm{M}$. Furthermore, as we add more angles from the first column to the M set, the number of nonnegative terms increases on the left-hand side of Eq. (D73). Then a smaller β_1 value will satisfy Eq. (D73). So, by comparing Eqs. (D70) and (D72) in this way, we can certify the left-hand-side inequality in (D71), whereas after a simplification, the right-hand-side inequality becomes $\theta_{i'1} + \theta_{it} \leqslant \pi$, which is true as every $\theta \leqslant \frac{\pi}{2}$.

In conclusion, the lower limit β' is the root of Eq. (D64) for every $1 \leqslant m \leqslant (d-1)$. The upper limit β'', for $m = 1$, is given by (D67) and can be derived from Eq. (D69). For $1 < m$, β'' is the solution of Eq. (D70). (D74)

In fact, Eq. (D69)—where two angles are taken from the first column in Θ—is also like Eq. (D73). Basically, one needs to solve an equation such as (D73)—where $2 \leqslant \mathrm{M} \leqslant d$ angles are picked from a row or a column in Θ—to get a limit and then an endpoint of an m-parametric curve. When $m = 1$ then M can only be 2 [see (D64) and (D69)]. And when $1 < m \leqslant (d-1)$, then M can be either m or $m+1$ [see (D70) and (D64)].

To solve Eq. (D73) for β_1, we transform it into

$$\mathbf{x}\,(\cos\beta_1)^2 + \mathbf{y}\,\sin\beta_1\,\cos\beta_1 + \mathbf{z} = 0, \quad \text{(D75)}$$

where

$$\mathbf{x} := \sum_{i=1}^{\mathrm{M}} \cos 2\theta_{i1} = 2\sum_{i=1}^{\mathrm{M}} r_{i1} - \mathrm{M}, \quad \text{(D76)}$$

$$\mathbf{y} := \sum_{i=1}^{\mathrm{M}} \sin 2\theta_{i1} = 2\sum_{i=1}^{\mathrm{M}} \sqrt{r_{i1}\,(1 - r_{i1})}, \quad \text{and} \quad \text{(D77)}$$

$$\mathbf{z} := \sum_{i=1}^{\mathrm{M}} (\sin\theta_{i1})^2 - 1 = \mathrm{M} - \sum_{i=1}^{\mathrm{M}} r_{i1} - 1. \quad \text{(D78)}$$

Calling $(\cos\beta_1)^2 = q_1$ by relations (3) and (4), we can write Eq. (D75) as

$$\mathbf{x}\,q_1 + \mathbf{y}\sqrt{q_1\,(1 - q_1)} + \mathbf{z} = 0. \quad \text{(D79)}$$

The two roots of Eq. (D79) are

$$(\cos\beta_1)^2 = q_1 = \frac{(\mathbf{y}^2 - 2\,\mathbf{x}\,\mathbf{z}) \pm \mathbf{y}\sqrt{\mathbf{y}^2 - 4\,\mathbf{z}\,(\mathbf{x} + \mathbf{z})}}{2\,(\mathbf{x}^2 + \mathbf{y}^2)}, \quad \text{(D80)}$$

which depend only on the M set $\{\theta_{11}, \ldots, \theta_{\mathrm{M}1}\}$ associated with Eq. (D73).

We pick the root, (D80), with a positive sign for the following reasons. First, for $\mathrm{M} = 2$, we have an equation such as (D72), and its root $\widetilde{\beta}$—given in (D71)—corresponds to the positive-sign solution [see also (D68) with (D69)]. Second, for $\mathrm{M} = d$, $\beta_1 = 0$ is the only permissible solution of Eq. (D73). This is because angles θ_{i1} are not random real numbers; they follow $\sum_{i=1}^{d} (\cos\theta_{i1})^2 = 1$. When $\mathrm{M} = d$, $\mathbf{z} = d - 2 = -\mathbf{x}$ [see (D76) and (D78)], and always the solution, (D80), with the positive sign provides $\beta_1 = 0$. Third, for a pair of MUBs [19], where every θ is the same $\arccos\frac{1}{\sqrt{d}}$, one can directly solve Eq. (D73). For every M set, we get the same β_1 [see χ in (56)], which corresponds to

$$(\cos\beta_1)^2 = \frac{[1 + \sqrt{(d-1)(\mathrm{M}-1)}]^2}{d\mathrm{M}}; \quad \text{(D81)}$$

this is clearly the root, (D80), with a positive sign.

[1] W. Heisenberg, Z. Phys. **43**, 172 (1927); English translation in [2].

[2] *Quantum Theory and Measurement*, edited by J. A. Wheeler and W. H. Zurek (Princeton University Press, Princeton, NJ, 1983), pp. 62–84.

[3] H. Weyl, *The Theory of Groups and Quantum Mechanics*, translated by H. P. Robertson (E. P. Dutton, New York, 1932), Chap. 2, Sec. 7 and Appendix 1.

[4] P. Busch, T. Heinonen, and P. Lahti, Phys. Rep. **452**, 155 (2007).

[5] H. P. Robertson, Phys. Rev. **34**, 163 (1929).

[6] D. Deutsch, Phys. Rev. Lett. **50**, 631 (1983).

[7] K. Kraus, Phys. Rev. D **35**, 3070 (1987).

[8] H. Maassen and J. B. M. Uffink, Phys. Rev. Lett. **60**, 1103 (1988).

[9] S. Wehner and A. Winter, New J. Phys. **12**, 025009 (2010).

[10] I. Bialynicki-Birula and Ł. Rudnicki, in *Statistical Complexity: Applications in Electronic Structure*, edited by K. D. Sen (Springer, Dordrecht, Netherlands, 2011), pp. 1–34.

[11] P. J. Coles, M. Berta, M. Tomamichel, and S. Wehner, Rev. Mod. Phys. **89**, 015002 (2017).

[12] W. K. Wootters, Phys. Rev. D **23**, 357 (1981).

[13] H. J. Landau and H. O. Pollak, Bell Syst. Tech. J. **40**, 65 (1961).

[14] G. B. Folland and A. Sitaram, J. Fourier Anal. Appl. **3**, 207 (1997).

[15] C. Niculescu and L.-E. Persson, *Convex Functions and Their Applications: A Contemporary Approach* (Springer-Verlag, New York, 2006).

[16] A. Lenard, J. Funct. Anal. **10**, 410 (1972).

[17] U. Larsen, J. Phys. A: Math. Gen. **23**, 1041 (1990).

[18] J. Kaniewski, M. Tomamichel, and S. Wehner, Phys. Rev. A **90**, 012332 (2014).

[19] T. Durt, B.-G. Englert, I. Bengtsson, and K. Życzkowski, Int. J. Quantum Info. **8**, 535 (2010).

[20] I. D. Ivanovic, J. Phys. A: Math. Gen. **25**, L363 (1992).

[21] J. Sánchez-Ruiz, Phys. Lett. A **201**, 125 (1995).

[22] M. A. Ballester and S. Wehner, Phys. Rev. A **75**, 022319 (2007).

[23] S. Wu, S. Yu, and K. Mølmer, Phys. Rev. A **79**, 022104 (2009).

[24] P. Mandayam, S. Wehner, and N. Balachandran, J. Math. Phys. **51**, 082201 (2010).

[25] A. E. Rastegin, Int. J. Theor. Phys. **51**, 1300 (2012).

[26] P. Busch, P. Lahti, and R. F. Werner, Phys. Rev. A **89**, 012129 (2014).

[27] A. J. M. Garrett and S. F. Gull, Phys. Lett. A **151**, 453 (1990).

[28] J. Sánches-Ruiz, Phys. Lett. A **244**, 189 (1998).

[29] G. C. Ghirardi, L. Marinatto, and R. Romano, Phys. Lett. A **317**, 32 (2003).

[30] G. M. Bosyk, M. Portesi, and A. Plastino, Phys. Rev. A **85**, 012108 (2012).

[31] J. I. de Vicente and J. Sánchez-Ruiz, Phys. Rev. A **71**, 052325 (2005).

[32] S. Zozor, G. M. Bosyk, and M. Portesi, J. Phys. A **46**, 465301 (2013).

[33] A. Peres, *Quantum Theory: Concepts and Methods* (Kluwer Academic, Dordrecht, Netherlands, 1995).

[34] Evidently, this paper only talks about preparation certainty and uncertainty relations.

[35] C. Tsallis, J. Stat. Phys. **52**, 479 (1988).

[36] R. T. Rockafellar, *Convex Analysis* (Princeton University Press, Princeton, NJ, 1970).

[37] A. Sehrawat, arXiv:1611.09760v2 [quant-ph].

[38] In [16], the region of allowed expectation values of a couple of orthogonal projectors (Q,P) is obtained as the convex hull of two ellipses. For $Q = |a\rangle\langle a|$ and $P = |b\rangle\langle b|$, the two ellipses become one, which is the same as ours. A pair of ellipses in [17]—associated with the two ellipses in [16]—specifies an allowed region for a pair of purities related to a pair of projective measurements. In [18], by taking M binary observables, an ellipsoid, inside a hypercube, is presented as the allowed region for the expectation values of the M observables. For $M = 2$, the ellipsoid becomes our ellipse.

[39] A. Rényi, in *Proceedings of the 4th Berkeley Symposium on Mathematical Statistics and Probability* (University of California Press, Berkeley), Vol. 1, pp. 547–561.

[40] L. Maccone and A. K. Pati, Phys. Rev. Lett. **113**, 260401 (2014).

[41] C. E. Shannon, Bell Syst. Tech. J. **27**, 379 (1948).

[42] A. Luis, Phys. Rev. A **84**, 034101 (2011).

[43] H. F. Hofmann and S. Takeuchi, Phys. Rev. A **68**, 032103 (2003).

[44] O. Gühne, Phys. Rev. Lett. **92**, 117903 (2004).

[45] O. Gühne and M. Lewenstein, Phys. Rev. A **70**, 022316 (2004).

[46] V. Giovannetti, Phys. Rev. A **70**, 012102 (2004).

[47] *Quantum State Estimation*, edited by M. Paris and J. Řeháček (Springer-Verlag, Heidelberg, 2004).

[48] W. Rudin, *Principles of Mathematical Analysis* (McGraw-Hill, Singapore, 1976), Chap. 2.